General Disclaimer

One or more of the Following Statements may affect this Document

- This document has been reproduced from the best copy furnished by the organizational source. It is being released in the interest of making available as much information as possible.

- This document may contain data, which exceeds the sheet parameters. It was furnished in this condition by the organizational source and is the best copy available.

- This document may contain tone-on-tone or color graphs, charts and/or pictures, which have been reproduced in black and white.

- This document is paginated as submitted by the original source.

- Portions of this document are not fully legible due to the historical nature of some of the material. However, it is the best reproduction available from the original submission.

GCA-TR-69-9-N

LUNAR LANDER MASS SPECTROMETER, PHASE II

Project Manager: Wallace S. Kreisman

GCA CORPORATION
Bedford, Massachusetts

FINAL REPORT
CONTRACT NO. NAS5-9393

PREPARED FOR
NATIONAL AERONAUTICS AND SPACE ADMINISTRATION
GODDARD SPACE FLIGHT CENTER
GREENBELT, MARYLAND

OCTOBER 1969

GCA-TR-69-9-N

LUNAR LANDER MASS SPECTROMETER, Phase II

April 1967 - December 1968

Final Report

Contract No. NAS5-9393

October 1969

Contracting Officer: J. Turner
Technical Monitor: I. Adler 644

Prepared by

GCA CORPORATION
GCA TECHNOLOGY DIVISION
Bedford, Massachusetts

Project Manager: Wallace S. Kreisman

for

National Aeronautics and Space Administration
Goddard Space Flight Center
Greenbelt, Maryland

TABLE OF CONTENTS

LUNAR LANDER MASS SPECTROMETER, PHASE II

By Wallace S. Kreisman
GCA Corporation, GCA Technology Division, Bedford, Mass.

SUMMARY

A breadboard miniaturized sputter source solids analysis mass spectrometer was designed, constructed and tested to determine its suitability as a lunar mass spectrometric probe. The instrument operated over the mass range of 1 to 100 amu in two segments and was capable of detecting as little as a few ppm of some impurity elements in solids. A low power Penning source was used to generate the primary ion beam. Electric and permanent magnet sector fields provided double focusing of secondary ions sputtered from the sample. Two separate electron multipliers detected the mass peaks. The design, construction and operation of the instrument is described.

INTRODUCTION

The Moon is one of the few bodies of the solar system that have preserved, at its surface, many of the basic features of its past history. This is due primarily to the absence of such effects as erosion by wind and flowing water. It is believed that many of the broad features of the Moon are more than four billion years old. If this is so, a detailed study of the lunar surface will yield information about the history and origin of the Moon and the entire solar system (ref. 1).

There are a host of scientific questions that will be answered when more is known about the chemical and mineral composition of the lunar material and its distribution on and below the surface. In order to aid in the identification of lunar materials in situ, a miniaturized solids analysis mass spectrometer has been designed, constructed, and tested.

The miniaturized solids analysis mass spectrometer is called a "lunar lander" mass spectrometer. This instrument uses a primary beam of positive ions to bombard the sample surface being analyzed. Many of the atoms and molecules of the sample surface are ionized and sputtered away from the surface. A small, double-focusing, magnetic deflection mass spectrometer is used to collect and analyze the sputtered ions from the sample.

The purpose of the design, development and test program reported herein was to create a miniaturized solids analysis mass spectrometer that would be compatible with the severe limitations on space, weight,

and electrical power imposed by a lunar mission. This instrument might be hand-carried on the Moon or else mounted on a roving vehicle.

The principles of operation of a sputter source type of solids analysis mass spectrometer are well known, although the details of the sputtering process are not known (ref. 2). The instrument to be described in this report was a variation of existing sputter source mass spectrometers. Some of the chief differences between the lunar lander and commercial sputter source mass spectrometers were as follows: (1) a Penning source was used in place of a duoplasmatron to generate the primary ion beam, (2) the angle of incidence of the primary beam at the target could be varied, (3) a permanent magnet was used in place of an electromagnet to separate ions of different mass, and hence, the accelerating voltage for the sputtered ions (i.e., the secondary ion beam) was varied to cover the mass range, (4) two mass ranges were used instead of a single mass range; however, the two mass ranges could be swept simultaneously, (5) the magnetic sector analyzer field followed the electric field energy selector, and (6) extraction of secondary ions from the target occurred normal to the target so that the secondary ion optics were axially symmetric.

The following chapters describe the design and construction of both the lunar lander mass spectrometer and its vacuum test system, the tests that were performed to investigate and optimize various parameters of the system, the results obtained from the aforementioned tests, and, finally, the conclusions reached.

EQUIPMENT DESIGN

Mass Spectrometer Design and Construction

General Description. - The lunar lander mass spectrometer was a complete, miniaturized, solids analysis mass spectrometer. In common with other mass spectrometers, it had three major basic components: an ion source, an analyzer section, and an ion detector. The ion detectors used with this mass spectrometer were well known, commerically available electron multipliers, and so there is little discussion of these units in this report. On the other hand, the sputter ion source and the analyzer section were unique components, and hence they are described in detail. Photographs of the lunar lander mass spectrometer mounted within the test chamber are shown in Figures 1 and 2.

A block diagram of the complete mass spectrometer is presented in Figure 3. The limitation on electrical power for this miniaturized space vehicle instrument excluded the use of an electromagnet for the magnetic sector mass dispersing field (mass analyzer). The use of a permanent magnet for the analyzer made it necessary to divide the total desired mass range of 1:100 atomic mass units (amu) into two separate mass ranges, a

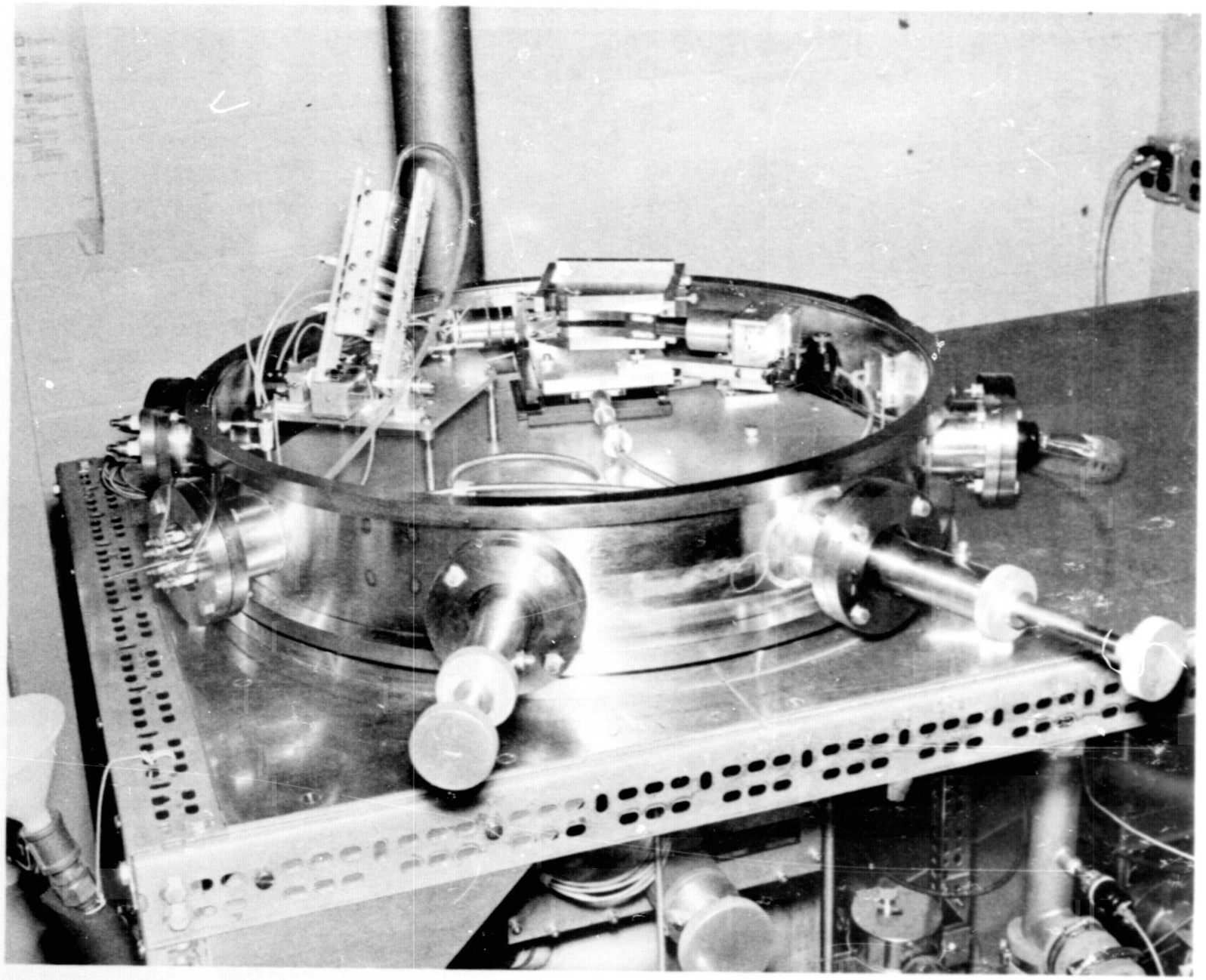

Figure 1. Photograph of the lunar lander mass spectrometer mounted within the test chamber, front view.

Figure 2. Photograph of the lunar lander mass spectrometer mounted within the test chamber, oblique view.

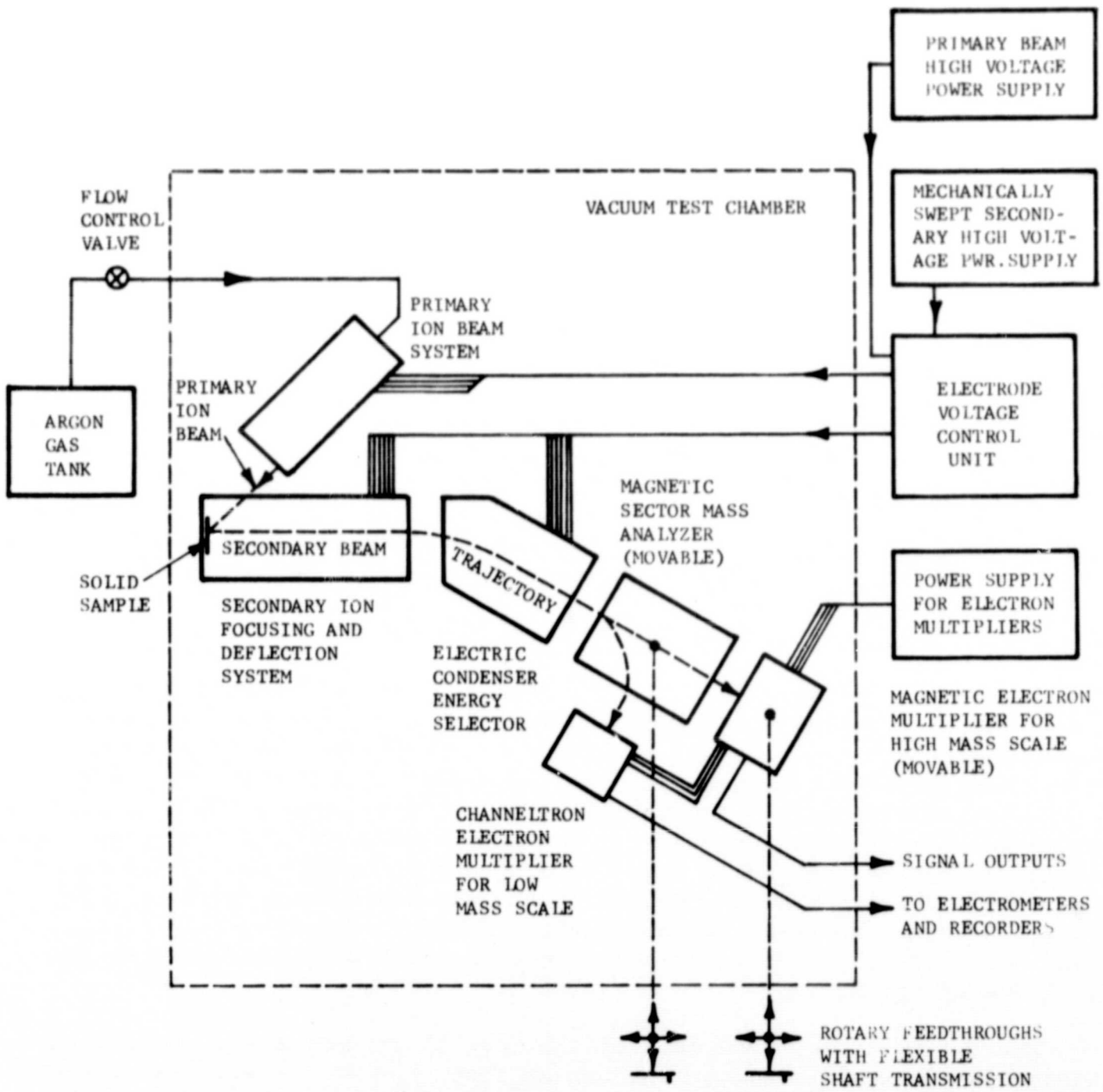

Figure 3. Schematic block diagram of lunar lander mass spectrometer.

low mass range from 1 to 10 or 12 amu and a high mass range from 10 or 12 to 100 amu. In laboratory type mass spectrometers, such a change in mass range is often accomplished by using separate permanent magnets, or by magnetically shunting a single magnet. In the lunar lander instrument, the change in mass range was accomplished by collecting the lighter low mass ions after they had traversed only a small portion of the total magnetic field. By using a second electron multiplier (a Channeltron electrostatic electron multiplier) and adjusting its position, it was possible to cover both mass ranges simultaneously with a single sweep of the secondary ion beam acceleration voltage.

As can be seen from Figure 3, the mass spectrometer was a tandem electric sector field (electric condenser) magnetic sector field instrument. The electric and magnetic fields were designed for double-focusing on the high mass scale to obtain maximum resolution for the higher masses. The electric field acted as an energy selector with a relatively narrow energy band pass. Ions having the same energy but different mass would then be separated by the magnetic sector field according to their momenta. As a final result, the trajectory of an ion in the magnetic sector was a function of its mass and the potential V through which it had been accelerated prior to entering the magnetic analyzer. By varying the secondary ion beam acceleration voltage V, all ion trajectories could be made to coincide with the trajectories leading to the ion detectors.

Looking at the overall system in Figure 3, it can be seen that the solid sample material was introduced into the vacuum of the instrument and positioned so that it was bombarded by the primary high energy argon ions. The primary ions generally had an energy of 6 kV and they caused a considerable amount of sputtering at the sample surface. Some of the atoms and molecules sputtered from the sample were ionized, and these so-called secondary ions could then be focused and formed into a secondary ion beam. Since the energy spread of the secondary ions could be quite large, a double focusing tandem electric field - magnetic field arrangement was used to obtain first order focusing of a divergent beam having a finite energy spread.

The entire ion-optical part of the mass spectrometer was mounted on a circular base plate within the vacuum test chamber. Electrical connections to the various primary and secondary beam electrodes were brought into the test chamber via vacuum tight ceramic-metal cable end seals mounted on several vacuum port flanges. The electrode voltage control unit consisted primarily of voltage divider chains and linear potentiometers that could be adjusted to vary the voltages of the different electrodes. All of the secondary optics electrodes used voltages that were derived from a well-regulated negative high voltage power supply whose output was varied (swept) mechanically with a motor driven control potentiometer. Positive high voltages for the primary beam system were obtained from a second well-regulated high voltage power supply. A third well-regulated high voltage power supply furnished the negative voltages

used to operate the two electron multipliers. The low level, dc output current signals were amplified by standard Keithley electrometers and displayed on an X-Y recorder.

Sputter Ion Source Primary Beam System. - The complete ion source for the lunar lander consisted of several elements. Primary beam ions (of argon or some other suitable gas) were formed in a Penning type cold cathode discharge source. These positive ions were then extracted from the discharge region and focused by an einzel or unipotential lens so that they formed a small spot at the sample.

Figure 4 is a schematic drawing of the primary beam system. The Penning source was located at the top of the lens system. Element (2) was the Penning source anode, while elements (1) and (4) formed the cathode. Element (3) was a two-piece sleeve or ring magnet that furnished a magnetic field within the source via the cathodes, which acted as magnetic pole pieces. The primary beam gas was admitted to the Penning source via the tube (14), and positive ions were extracted from the source through the small hole (0.080 inch diameter x 0.025 inch long) in the aluminum liner of the lower cathode. The extraction electrode (5) created a strong enough field to draw ions out of the source, and the three element primary einzel lens (elements (6), (7), and (8)), focused these ions to a small spot on the sample which was placed in contact with the sample holder (9). Space was provided for the insertion of primary beam centering electrodes (16), but it was not necessary to use such electrodes since the entire primary beam optics could be moved mechanically with respect to the fixed position of the sample holder by means of the mounting blocks (10). The primary beam optics could also be rotated about the horizontal axle that passed through the mounting block bearings. This rotational motion changed the angle between the impinging primary beam and the sample surface.

The Penning source cathodes were operated at the full primary beam positive voltage. The Penning source anode was operated at about 500 to 1000 volts positive with respect to the cathodes. The anode to cathode potential could be varied smoothly from zero to about 1000 volts by means of a Variac located in the electrode voltage control unit. The primary beam ion voltage had some value greater than the primary beam positive voltage since the sample was maintained at zero or ground potential. The extraction electrode was generally operated a few thousand volts negative with respect to the source cathode. The two outer electrodes of the einzel lens were maintained at ground potential, while the center electrode (7) was kept at a positive potential to yield a "Decel-accel" lens (so-called because the beam is decelerated in the first gap and accelerated in the second gap). Such a lens provides a strong focusing effect over a short distance. The extraction electrode (5) could be varied in potential to change the intensity of the ion beam without appreciably affecting the focusing of the beam. At the same time, the division of the ion acceleration region between the source cathode and the

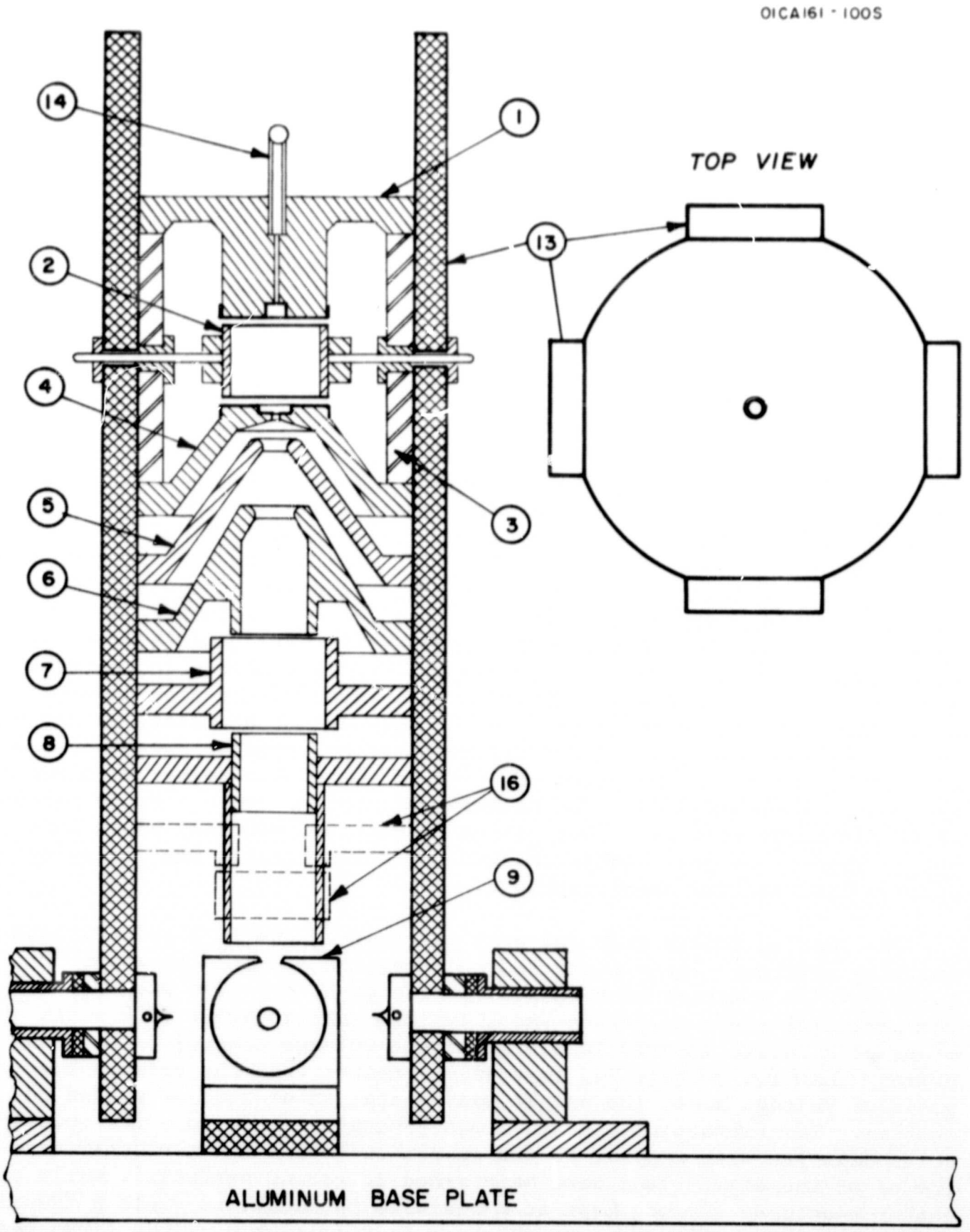

Figure 4. Schematic of lunar lander mass spectrometer primary ion beam system.

first electrode of the einzel lens into two separate acceleration regions, tended to decrease the chance of arcing between the source and the extraction electrode.

The voltages applied to the extraction and focus electrodes were obtained from the electrode voltage control unit. The potential for each of these electrodes was variable in four separate ranges from zero to the full primary beam acceleration voltage. Each range, in turn, was subdivided into ten steps.

All of the electrodes of the primary beam optics, together with the Penning source, were fastened between four long rectangular strips of Aremcolox 502-600 machinable ceramic element (13). The sleeve magnets were 6 cm in diameter and 6 cm long and could provide a maximum magnetic induction in the gap between the pole pieces (cathodes) of 1400 gauss. The magnets weighed 550 grams.

The Penning source was a scaled-down version of a similar source that was developed for the first phase of the lunar lander project. The original source was described in detail in the final report for this phase (ref. 3).

Unique features of this Penning source were the counterbores at the centers of both the upper and lower cathodes, the use of aluminum liners to cover the Armco mild steel cathodes, and a relatively long cylindrical aluminum anode to enclose the space between the cathodes. The counterbores in both cathodes produced an inhomogeneity in the magnetic field. This resulted in an increase in the electron density along the central axis, and thus increased the extracted ion current. The aluminum liners on the cathodes minimized sputtering within the discharge. Such sputtering action could coat the source insulators, which were deliberately placed behind the anode to minimize this occurrence. The extra long anode cylinder more effectively confined the discharge and thus increased the discharge intensity.

Experiments made with this source showed that one could expect regions of source instability (plasma oscillations, etc.) if the magnetic field was sufficiently high, say 800 gauss or greater, for discharge currents between approximately 6 to 30 mA. For smaller magnetic fields and for discharge currents either less than 6 mA or greater than 30 mA, the Penning source discharge was stable.

When the experimental Penning source was used with the laboratory solids mass spectrometer, the spectra obtained were comparable to those obtained with the standard duoplasmatron source. An analysis of the primary beam constituents showed that the major contaminant was either N_2 or CO in the amount of 4 parts per thousand. Additional contaminants were H_2O, O_2, H_2, Aℓ, Hg, H, N, and O and some faint indications of hydrocarbon. The contamination with aluminum was less than 100 ppm.

The advantages of the Penning source over that of the standard laboratory duoplasmatron source were that it had no filament, consumed less power and was simpler in construction. The disadvantages were its relatively high internal sputtering, the wider spread in ion energies, and lower efficiency.

All of the accelerating and focusing electrodes of the primary beam system were made of aluminum, with the exception of cylindrical insert (8) of the lower (exit) element of the einzel lens. The use of aluminum decreased the instrument weight and minimized sputtering. Element (8) was made of 303 stainless steel. Electrode edges were rounded and polished to minimize corona and arcing. Wherever possible, the electrodes were designed to "nest" or "overlap" so that the primary ion beam could not "see" any of the insulators that supported them. The reason for doing this was to eliminate the perturbing effect of varying insulator charge-up on the ion beam. Element (17), as shown in Figure 3, shielded the ion beam in its traversal between the einzel lens and the sample.

The potentials to be applied to the extraction electrode and the center element of the einzel lens (the outer elements were at zero or ground potential) were to be determined experimentally. Voltage divider chains of resistors providing a wide range of potential were provided in the electrode voltage control unit for this purpose. The control unit is described in a later section.

It might be said that a study of the focusing characteristics of a typical einzel lens shows that for the decel-accel configuration, the potential of the center element must be greater than about one half the total accelerating potential of the ions if there is to be focusing in a relatively short distance. The magnification of the object (in this case the 0.080 inch or 2 mm diameter of the cathode aperture) was approximately unity for the primary beam system. The included beam angle was effectively determined by the aperture. According to the scaled drawings, the beam half-angle was about 20 degrees at the extraction electrode. The extraction electrode and the top outer electrode of the einzel lens actually formed a so-called "aperture lens" which could act to either focus (positive lens) or defocus (negative lens) the positive ions. If the extraction electrode potential was about 1/3 of the positive primary beam acceleration voltage applied to the source cathode, and the top outer electrode of the einzel lens was at zero potential, the potential drop between the cathode and extraction electrode was greater than the drop between the extraction electrode and einzel lens electrode. This arrangement led to a negative aperture lens, that caused the ion beam to diverge as it entered the einzel lens. The einzel lens had enough power to refocus the divergent beam, however. The advantage of having a low potential on the extraction electrode was that more ions were drawn out of the Penning source discharge.

Since the primary optics system consisted wholly of cylindrical lenses, the primary beam was axially symmetric. However, the axis of the primary

beam system was adjusted to a fixed position making an angle of 53.5° with the horizontal, so that the beam would strike a vertical sample with an angle of incidence of 53.5°. The intersection of the cylindrical primary beam with the plane sample surface thus formed an elliptical spot. The minor diameter of the ellipse was equal to the primary beam diameter D, while the major diameter of the ellipse was (1/cos 53.5°) D or 1.68 D in the vertical direction. The elongated nature of the elliptical spot at the sample was used to advantage by placing all the slits of the secondary optics beam system in the vertical direction.

Secondary Ion Beam System. -

General description: The secondary ion beam system consisted of the following major elements: (1) sample holder and a sample charge neutralization filament, (2) electrodes to focus and deflect (position) the positive ions sputtered from the sample, (3) shielded entrance and angle slits to define the beam size, (4) an electric condenser (to provide a cylindrical electric field) with field terminating shunt plates and focusing matsuda plates followed by an energy slit to define the energy spread of the ions and provide double focusing in combination with the magnetic sector field, (5) vertical beam focusing electrodes, (6) the magnetic sector field to separate ions of various masses, (7) magnetic entrance and exit shunts to limit the extent of the magnetic field, (8) a shielded exit slit to separate the various ion masses, (9) a post acceleration focusing plate, (10) a magnetic electron multiplier for the high mass scale, and (11) a Channeltron electrostatic electron multiplier for the low mass scale.

Figure 5 shows the general arrangement of the electrodes of the secondary ion beam system. This drawing is not to scale and is only meant to identify the various electrodes and components.

All of the elements to the left of the magnetic sector field were mounted on an insulated planar surface to simplify the alignment problem. The insulation used between the surface and the sample holder and focusing deflection electrodes was aremcolox 502-600 machinable ceramic. The electric condenser assembly was mounted on this plate by three insulating nylon screws. The plate itself was mounted on the circular base by four adjustable standoffs. Some of the individual electrodes adjacent to the electric condenser were separated and centered relative to one another by either pyrex glass spheres or teflon spacers. Most of the electrodes were made of either 304 stainless steel or nickel plated low carbon steel with the notable exception of the sample holder, which was made of tantalum to minimize sputtering contamination.

The magnet pole pieces and magnet shunts were made of Armco soft iron. All of the brackets and mounting plates were made of aluminum. The magnet assembly was mounted on a Gaertner Model M326 two-coordinate positioning stage via an insulating teflon plate so that the magnet (and

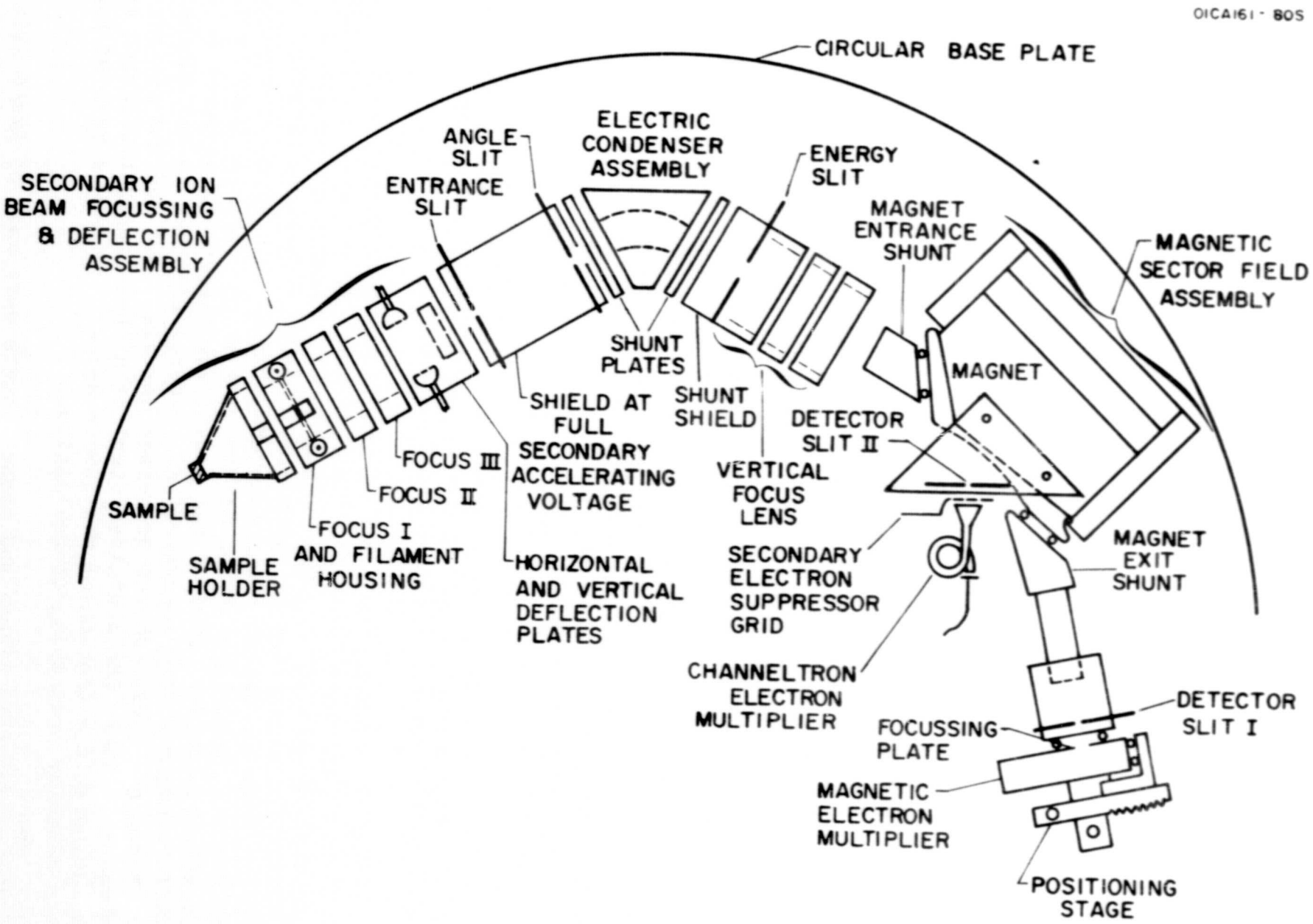

Figure 5. Schematic of Lunar lander mass spectrometer secondary ion beam system.

the attached ion detector assemblies) could be moved relative to the ion beam emerging from the electric condenser assembly. The coordinate stage was fastened directly to the circular base plate. The magnetic electron multiplier used with the high mass scale was also mounted on a two-coordinate positioner attached to the movable magnet assembly so that it could be moved relative to the ion beam emerging from the magnet. The low mass scale Channeltron electron multiplier was fixed in position.

Since the Penning ion source for the primary ion beam was at a high positive potential and the sample holder and sample being analyzed were kept at zero or ground potential, the secondary ion beam acceleration voltage V had to be negative with respect to ground. All of the secondary beam electrodes had to be well-insulated from ground in order to impose a minimum current drain on the secondary voltage power supply. Since the focal lengths of all electron optical lenses depend on the voltage ratios of the various elements, it was necessary to design the electrode voltage control unit with voltage dividers to preserve the various voltage ratios as the secondary acceleration voltage V was swept over its entire range.

The electron multipliers that served as ion detectors also operated with high negative potentials (between approximately 1.5 and 3.0 kV) applied to their input ends. The output ends of the multipliers were effectively at zero or ground potential.

Secondary ion focusing and deflection: High energy primary beam ions striking the sample surface caused atoms and molecules of this surface to be sputtered in all directions. Since the primary ion beam energy was relatively high, there would be a significant number of positive ions formed from the sample material. These so-called "secondary ions" from the sample would be emitted in all directions with some characteristic distribution of velocities or energies. The secondary ion beam system, containing an electric and magnetic analyzer, was designed to extract, focus and mass analyze the secondary ions. Before describing the design of the secondary beam system in detail, there will be a brief discussion of the sputtering process that occurred at the sample.

The sputter source type of solids analysis mass spectrometer is based on the physical phenomenon of the sputtering of solid surfaces by the impingement of energetic ions. It has been found experimentally that a small percentage of the atoms and molecules that are released from the solid surface are ionized. According to one theory, the ratio of the sputtered ions to sputtered neutrals is given by the Langmuir-Saha formula (ref. 4).

$$N^+/N^o = \exp[11606\ (W-I)/T] \qquad (1)$$

where W is the work function of the solid in electron volts, I is the ionization potential in electron volts, and T is a highly localized "apparent temperature" measured in degrees Kelvin.

According to Equation (1), it must be expected that atoms with low ionization potential produce relatively more ions than atoms with high ionization potential and thus the sensitivity for each element will be different.

Theoretically, if one knows the number of sputtered neutrals, N^o, Equation (1) could be used to calculate the total secondary positive ion yield.

The sputtering ratios or sputtering yields for the total number of neutral atoms and ions removed from a solid per incident bombarding ion has been measured by many investigators (ref. 5).

It has been determined that for higher energies of the bombarding ions, the calculations of Rol (ref. 6) are the only ones that can explain the greater part of the observations of sputtering yields. Rol assumed that the sputtering ratio was proportional to the energy dissipated by the bombarding ion in the first atomic layers. The chance that a collision takes place near the surface is inversely proportional to the mean free path λ, so that the sputtering ratio can be written as

$$S = K \frac{E}{\lambda} \frac{M_1 M_2}{(M_1+M_2)^2} \text{ atoms/ion} \qquad (2)$$

where E = energy of the bombarding ion

M_1, M_2 = mass numbers of ion and target atoms

K = a constant for a certain combination of ion and target material

It is found experimentally that

$$K = a \exp\left(\frac{- b \sqrt{M_1}}{M_1+M_2} E_B\right) \qquad (3)$$

where E_B = binding energy of the target atoms

a, b = constants

With numerical values for a and b and expressing λ by means of the collision diameter R, Almen and Bruce (ref. 7) derived the expression

$$S = 4.24 \times 10^{-10} n_o R^2 E \frac{M_1 M_2}{(M_1+M_2)^2} \exp\left(- 10.4 \frac{\sqrt{M_1}}{(M_1+M_2)} E_B\right) \text{ atoms/ion} \qquad (4)$$

where E_B and E are given in electron volts, M_1 and M_2 in mass numbers, R in meters and n_o in meter^{-3}, the number of atoms per unit volume of the target material. This equation is restricted to perpendicular beam incidence. No simple expression can be obtained for oblique incidence (ref. 8).

There are deviations from Equation (4) that are greater than can be explained by experimental errors of the sputtering ratios and of the binding energies. For magnesium, aluminum and uranium and a few other metals that are covered with a thick oxide layer, sputtering ratios can be calculated only to an order of magnitude.

The sputtering ratios S of the elements for an impinging 10 keV argon ion beam vary from about 0.5 atom/ion for silicon to about 3.0 atoms/ion for silver -- a range of 1 to 6. This is actually a relatively narrow range (ref. 5). The range of measured positive ion yields γ^+ of the elements, when bombarded with a 10 keV argon ion beam, has a much greater spread, varying from a minimum of about 0.12×10^{-2} ion/argon ion for gold to a maximum of about 12×10^{-2} ion/argon ion for aluminum - a range of 1 to 100. The secondary ion yields γ^+ for the elements correlates fairly well with the reciprocal of their ionization potentials within various periods of the periodic table (ref. 9).

Any sputter source solids analysis mass spectrometer will exhibit a unique sensitivity for each element that is based partly on the various parameters that have just been discussed. However, in addition to these parameters, it must be recognized that the number of secondary ions from the sample surface that are collected and measured will depend on such other factors as the angular and energy distribution of the ions from the surface, the collection efficiency of the secondary ion optics near the sample, the transmission characteristics of the secondary optics (which will vary with the accelerating potential), the energy band pass or "window" of the electric condenser that permits only a varying fraction of the total number of ions of each mass to pass, and the conversion efficiency of the electron multiplier first dynode for each mass. In the last analysis, sensitivities for each element can only be determined experimentally.

The arrangement of the secondary ion beam system electrodes in the vicinity of the sample resembled that of the image converter tube. The sample holder surface (equivalent to the cathode of the image converter) was curved to form a cathode lens and minimize aberrations of the image. A series of three cylinder lenses, labelled focus I, focus II and focus III, respectively, extended from the cathode lens toward the entrance slit of the electric analyzer.

Depending on the voltages applied to the focus electrodes it was possible to use these electrodes in different ways to focus the sample spot onto the entrance slit. The focus I electrode potential was invariably kept close to the sample zero potential. It was normally

slightly negative with respect to the sample by either a fixed or variable amount (that is, it could be a small percentage of the negative acceleration voltage). The focus II electrode could be operated at a large negative potential while the focus III electrode would be near zero potential. This was a typical einzel lens arrangement of the accel-decel type. A second way of operating the three focusing electrodes was to maintain the first focus electrode near zero (sample) potential, the second electrode at an intermediate value of negative potential and the third electrode at a high negative potential. This was equivalent to the immersion lens arrangement of an electron gun with the focus I electrode acting as the control grid, focus II electrode acting as the accelerating electrode or first anode, and the focus III electrode acting as the focusing electrode or second anode. Finally, a third way of operating the electrodes was to keep the focus I electrode near zero potential and have both the focus II and focus III electrodes kept at the same high negative potential. This was basically a two-cylinder type focusing lens arrangement. The spot on the sample was imaged at the entrance slit in each case with approximately unity magnification. In all three lens arrangements, there was undoubtedly a cross-over of the ion beam at or beyond the focus I electrode. The virtual image of the cross-over was then focused onto the entrance slit. The diameter of the ion beam at the cross-over point would vary with the initial energies of the secondary ions released from the sample. The potential of the three focusing lenses could be varied in twenty steps from ground potential to the full negative secondary accelerating voltage. The focusable lateral component of ion energy at the sample depended on the geometry of the lens system and the accelerating voltage. All ions which left the center of the sample and which moved within a conical region coaxial with the secondary optics axis and which had a half angle α', entered the entrance slit. The angle α' was determined approximately by the square root of the potential ratio and the angular acceptance half angle α of the mass spectrometer. If, for example, $\alpha = 1^{o}$ and $\sqrt{V_2/V_1} = 5$, one would expect to have $\alpha' \cong 5^{o}$. Here V_1 is the potential of the first focus electrode and V_2 is the potential of the second focus electrode. Ions could then have a maximum lateral or transverse component of energy determined by the relationship.

$$\frac{v_T}{v_A} = \frac{\sqrt{V_T}}{\sqrt{V_A}} = \tan \alpha' \qquad (5)$$

where v_T and V_T were the transverse velocity and corresponding transverse energy of the ion expressed in electron volts, and v_A and V_A were the axial velocity and the corresponding axial (acceleration) potential of the ion within the three element focus lens. The potential V_A could be taken to be equal to V_2, the potential of the second focus electrode, which, in turn, would be some fraction γ of the total secondary ion beam acceleration voltage V. One could then write the following expression:

$$V_T = \gamma \tan^2 \alpha' \, V \qquad (6)$$

If $\gamma = 0.75$, a representative value, and $\alpha' = 5^\circ$ so that $\tan^2 \alpha' \cong 0.008$, then

$$V_T \cong 0.006 \, V \qquad (7)$$

It will be shown later that the cylindrical electric condenser passed only positive ions having initial axial energies of about 0.01 V with the energy slit employed. These two conditions determined the ion velocity distribution at the sample which would be accepted and analyzed by the mass spectrometer. Ions having greater initial energies (velocities) in the axial and transverse directions would not contribute to the output signal. As the secondary acceleration voltage increased, the range of values of acceptable initial ion energy also increased and thus more ions contributed to the output signal. Changes in the focusing of the sample spot on the entrance slit with changes in the accelerating potential were expected to be negligible since the focus I, II and III electrode potentials were maintained at a constant ratio. The focus could be changed by maintaining the charge neutralization filament (located within the focus I electrode) at a constant potential with respect to the sample.

The sample charge neutralization filament was fashioned out of a loop of twelve mil diameter thoriated tungsten wire. This loop was concentric with the optic axis and had a diameter of approximately 1/2 inch within the 3/4 inch diameter aperture of the focus I electrode. The current to the filament could be varied by means of a filament current control located within the electrode voltage control unit. Of course, the filament current determined the filament temperature and electron emission. A filament bias control was also provided within the control unit that could provide negative bias voltages up to a few hundred volts.

Samples of insulating material (dielectrics) would normally be charged positively at their surface by the positive ion primary beam. This positive charge had to be neutralized or else secondary ions leaving the sample would have an "effective high initial energy" and could not pass through the electric condenser.

The vertical deflection and horizontal deflection plates were contained within a single electrode housing. The deflection plates and housing were made of mild steel, and aremcolox 502-600 machinable ceramic was used for the four insulating plates to which the four deflection plates were mechanically attached via threaded rods that passed through clearance holes in the housing. The secondary ion beam would first be deflected by the horizontal deflection plates before entering the vertical deflection plates. The deflection plates were 3/8 inch long by 1/2 inch wide and were spaced approximately 3/8 inch apart. The potential of the lower vertical deflection plate, one of the horizontal deflection plates and

the housing was maintained at a constant level of about 75 percent of the acceleration voltage. The potentials of the upper vertical deflection plate and the remaining horizontal deflection plate could be varied independently in 20 steps from 50 to 100 percent of the acceleration voltage.

Mass analyzer ion optical design: The analyzer ion optical design parameters are shown in Figure 6. This figure should be studied together with Figure 5, which shows the actual arrangement of the various elements. The ion optical system begins with an entrance slit S' followed by a beam angle limiting slit S_α, an electric sector condenser of radius a_e and sector angle ϕ_e, a beam energy limiting slit S_E, a magnetic sector of radius a_1 and sector angle ϕ_1 providing a beam entry angle θ_1', a beam exit angle θ_1'' and an exit slit S_1'' for the high mass scale. A small portion of the total magnet of radius a_2 and sector angle ϕ_2 provides an exit angle θ_2'' leading to the exit slit S_2'' for the low mass scale.

Important quantities that must be determined for the analyzer ion optical system are the object distance ℓ_e' and image distance ℓ_e'' of the electric condenser, the object distance ℓ' and the two image distances ℓ_1'', and ℓ_2'' for the magnetic sectors, and the resolution of the instrument for both mass scales.

The design of the mass spectrometer made use of the theory developed by Mattauch and Herzog (ref. 10). Other elements of the design are covered by Ewald and Hintenberger and others (ref. 11-17).

The basic equation for the radius of curvature a_m for a singly-charged ion in a homogeneous magnetic field of strength H gauss is

$$a_m = 143.6 \frac{\sqrt{MV}}{H} \text{ cm} \qquad (8)$$

where M = atomic mass number (amu)

V = secondary beam accelerating voltage (volts)

H = magnetic field in gauss

a_m = radius in cm

On the basis of a magnetic field strength of 1750 gauss and a secondary acceleration potential V that varied between 300 and 3000 volts, the total mass range from 1 to 100 amu could be covered in two mass ranges: a high mass range from 10 to 100 amu using an ion trajectory of radius $a_1 = 14.00$ cm, and a low mass range from 1 to 10 amu using an ion trajectory of radius a_2 equal to $14.00/\sqrt{10} = 4.43$ cm.

Having determined the ion trajectory radii, the next step in the design was to use the double focusing condition written below to determine such parameters as the electrostatic field image distance ℓ_e'' and

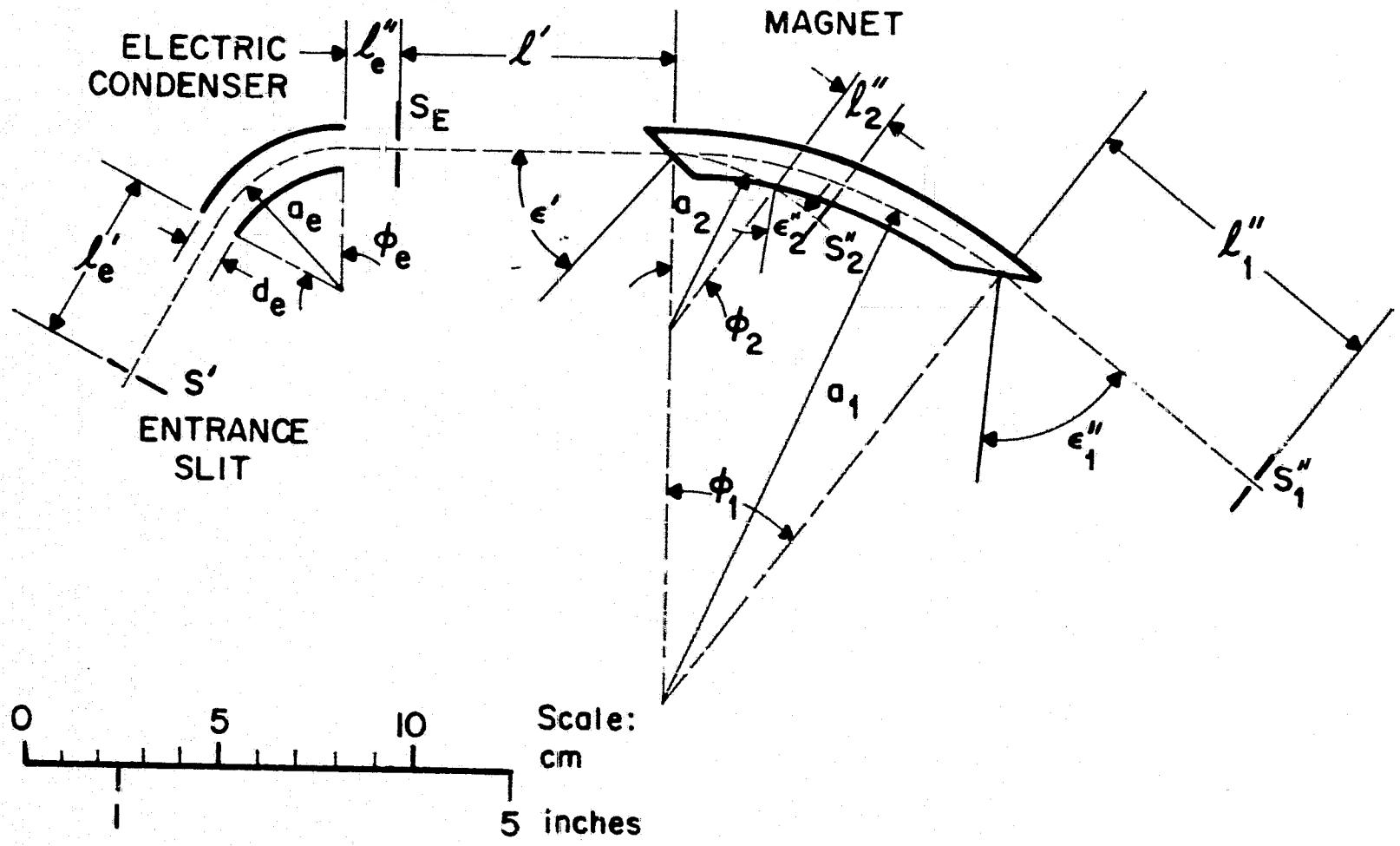

Figure 6. Analyzer ion optical design parameters of the lunar lander mass spectrometer.

the magnetic field object distance ℓ':

$$K' = K''_e$$

or

$$a(1-\cos\phi) + \ell'[\sin\phi + (1-\cos\phi)\tan\theta'] = a_e(1-\cos\sqrt{2}\,\phi_e) + \ell''_e\sqrt{2}\sin\sqrt{2}\,\phi_e \quad (9)$$

where K' and K''_e are the magnetic and electric dispersion coefficients, respectively. Values for the magnet sector angle ϕ, the magnet beam entry angle θ', the electric condenser radius a_e and the condenser sector angle ϕ_e were selected to minimize the size of the instrument while maintaining sufficient resolution. In practice, this meant that several selections were made and the final results of these selections were determined. Thus, by using a technique of successive approximations, final values of all parameters were determined.

As mentioned earlier, the double focusing condition (ref. 9) was applied only to the high mass scale. The low mass scale optics were designed for standard first order magnetic focusing. The final values of the important ion optics design parameters are summarized in Table I.

TABLE I

LUNAR LANDER MASS SPECTROMETER ION OPTICS
DESIGN PARAMETERS

Electric Sector	High Mass Magnetic Sector	Low Mass Magnetic Sector
$a_e = 3.67$ cm	$a_1 = 14.00$ cm	$a_2 = 4.43$ cm
$\phi_e = 63.6^\circ$	$\phi_1 = 37.5^\circ$	$\phi_2 = 50.5^\circ$
$\ell'_e = 4.55$ cm	$\epsilon' = -45^\circ$	$\epsilon' = -45^\circ$
$\ell''_e = 1.48$ cm	$\epsilon''_1 = -60^\circ$	$\epsilon''_2 = -55^\circ$
$d_e = 0.80$ cm	$\ell' = 7.17$ cm	$\ell' = 7.17$ cm
	$\ell''_1 = 8.62$ cm	$\ell''_2 = 1.01$ cm

Spacing between the electric sector (condenser) and the magnetic sector is $\ell''_e + \ell' = 8.65$ cm. Spacing between the entrance and the angle slits is 3.60 cm.

The resolution for the two mass scales is found in terms of the lateral magnification and velocity dispersion of the electric sector and the lateral magnification and mass dispersion of the magnetic sector. The electrostatic sector field produces a real image of the entrance slit of width S′ at the image distance ℓ''_e. The size of this image (i.e., the width normal to the direction of the beam) is given by the equation

$$S''_e = M_{e\ lat}\ S' \tag{10}$$

where

$$M_{e\ lat} = -\ 0.570 \tag{11}$$

The velocity dispersion of the electric sector field is given by the equation

$$d = \beta\ K''_e \tag{12}$$

Here K''_e is called the velocity dispersion coefficient and d gives the distance between focal points for particles of energies eV (1+β) and eV (1-β), that is, for ions whose energies differ by 2β eV. Since $\beta = \Delta v/v$; $2\beta = \Delta V/V$.

The volt energy spread $\Delta V/V$ permitted by a slit of width S_E at the image point of the electric sector field is

$$\Delta V/V = 2S_E/K''_e \tag{13}$$

From the known design parameters, one calculates

$$\Delta V/V = 0.347\ S_E\ (S_E \text{ in cm}) \tag{14}$$

The intermediate image S''_e which the electric sector produces of the entrance slit is then imaged by the magnetic sector. The width S″ of this image is given by the expression

$$S'' = M_{m\ lat}\ S''_e \tag{15}$$

where

$$M_{m\ lat} = 0.87517 \text{ high mass scale} \tag{16}$$

$$M_{m\ lat} = 0.41142 \text{ low mass scale}$$

The effect of the electric and magnetic sectors in series is to give a combined magnification

$$M_{lat} = M_{e\ lat} \cdot M_{m\ lat} \tag{17}$$

or

$$M_{lat} = 0.49885 \text{ high mass scale} \tag{18}$$

$$M_{lat} = 0.23451 \text{ low mass scale}$$

When the double focusing condition is not satisfied, as is the case for the low mass scale, the first order resolution of the instrument can be written as

$$\left|\frac{M}{\Delta M}\right| = \frac{K''/2}{|S'\ M_{lat}| + S'' + |\beta\ K''|} \tag{19}$$

where K'' is the dispersion coefficient of the magnetic sector, S' is the entrance slit width, S'' is the exit slit width, M_{lat} is the combined transverse magnification of the electric and magnetic fields in tandem, and $\beta = \Delta v/v = (1/2)\ \Delta V/V$ is the velocity spread or one half the voltage (energy) spread of the ion beam. This equation permits one to assess the manner in which the entrance, exit and energy slits affect the resolution.

Neglecting for the moment the fact that there is double focusing for the high mass scale, Equation (19) leads to the following results:

High mass scale:

$$\left|\frac{M}{\Delta M}\right| = \frac{2.5272}{0.39885\ S' + S''_1 + 0.87694\ S_E} \tag{20}$$

Low mass scale:

$$\left|\frac{M}{\Delta M}\right| = \frac{0.9329}{0.23451\ S' + S''_2 + 0.32372\ S_E} \tag{21}$$

Equation (21) is exact for a first order calculation of the low mass scale resolution (all slit widths expressed in cm). Equation (20) yields a close approximation to the resolution of the doubly-focused high mass scale. In a more exact expression, the term involving S_E vanishes since the energy dispersion of the beam has been exactly counteracted by the magnetic dispersion. However, in the place of the S_E term, one must write the sum of the absolute values of all the optical aberrations

$$\sum_i |A_i| = a\, B_{11}\, \alpha^2 + a\, B_{12}\, \alpha\, \beta + a\, B_{22}\, \beta^2 \qquad (22)$$

It can be seen that these aberrations vary directly with the magnetic field radius "a", the beam divergence of half angle α and the velocity spread β.

Expressions for the coefficients B_{11}, B_{12} and B_{22} are given in the literature. The three terms on the right in Equation (22) are called the aperture defect, the astigmatism, and the chromatic defect, reading from left to right.

The values of the coefficients B_{ij} for the case of straight boundaries at the entrance and exit of the magnetic sector are

$$B_{11} = 7.93; \quad B_{12} = 11.97; \quad B_{22} = 7.89 \qquad (23)$$

The beam half angle α can be calculated from the widths of the entrance and angle slits and the spacing of 3.60 cm between these slits. For example, if the entrance and angle slits are each 0.0254 cm (0.010 inch) wide, the angle α is 26' or 0.00757 radians. If the energy slit S_E = 0.0254 cm also, then $\beta = 4.41 \times 10^{-3}$ and

$$\sum_i |A_i| = 1.414 \times 10^{-2}$$

In this case, the aberration addition to the line width is less than the equivalent energy spread addition of 2.227×10^{-2} of Equation (20), the calculated resolution for the high mass scale (which assumes complete separation of adjacent mass peaks) is 48.4. In terms of the resolution at the half peak height, this would be about 97.

Equation (21) can be used directly to calculate the resolution for the low mass scale. If $S' = S_E = 0.0254$ cm and $S_2'' = 0.0508$ cm (0.020 inch), the low mass resolution should be 16.2. However, the actual low mass resolution is expected to be much poorer than this because the low mass ion beam passes through a considerable segment of magnetic field near the magnet edge where there is a strong magnetic field gradient.

Another matter of importance in the ion optical design of the mass spectrometer was the consideration of both magnetic and electric fringing fields. The fringe field of the magnetic sector can act on the positive ion trajectories in three ways:

(1) It causes an additional deflection of the ion paths through the main magnetic field.

(2) It shifts the focus normal to the main trajectory.

(3) It shifts the focus parallel to the main trajectory.

It has been shown by Herzog that if properly dimensioned shunts are used, the actual magnetic field can be replaced by an "ideal field" which extends to a distance into the field free region (ref. 15).

If

$K = 6.35$ mm = spacing between magnet pole faces

$B = 4.50$ mm = spacing from top to bottom of shunt aperture

$d = 3.00$ mm = distance from shunt to magnet

and

$$D = 1.22 \text{ mm} = \sqrt{K^2 + d^2},$$

then the ideal field extends to a distance $\eta = 0.95$ mm from the straight pole faces. This field extension effectively increases the magnetic sector angles ϕ_1 and ϕ_2. The values of the lateral and longitudinal shifts of the focus for the high mass scale trajectory are:

$$\begin{aligned} \Delta b' &= 0.028 \text{ mm} = \text{lateral shift at the entrance boundary} \\ \Delta b'' &= 0.056 \text{ mm} = \text{lateral shift at the exit boundary} \\ \Delta \ell' &= -0.056 \text{ mm} = \text{longitudinal shift at the entrance boundary} \\ \Delta \ell'' &= -0.194 \text{ mm} = \text{longitudinal shift at the exit boundary} \end{aligned} \tag{24}$$

All of the magnetic fringe field effects listed above are small and can easily be compensated for by adjusting the position of the magnet and the electron multiplier ion detector.

The fringing electric field of the electric sector (condenser) was also limited in extent by placing electrostatic shunt plates adjacent to the entrance and exit boundaries (ref. 17). The dimension of the shunt plate aperture and its spacing from the boundaries was chosen to obtain an ideal electric field that extended a distance $\xi = 0.040$ cm from the actual condenser boundaries. This field extension effectively increased the electric sector angle by 1.26° (a 2 percent increase). The effect of the sector angle increase is to shift the position of the entrance slit relative to the condenser boundary from its initial design value of 4.55 cm to 4.77 cm assuming that the image distance of $\ell_e'' = 1.48$ cm remains unchanged. On the other hand, if $\ell_e' = 4.55$ cm is maintained constant, the value of ℓ_e'' will be reduced from 1.48 to 1.43 cm and the spacing

between the electric sector and the magnetic sector will be reduced accordingly. Since the magnet can be moved easily, this effect can be compensated.

Included in the ion optical system were additional elements that permitted the secondary ion beam to be focused in the vertical direction. The electric sector field had two electrically insulated flat electrode "Matsuda field plates" positioned above and below the inner and outer electric sector cylindrical electrodes (ref. 18). The two Matsuda plates were connected together and could be adjusted in potential. If this potential was the same as the potential of the median plane through which the ions passed, the focal distance of the electric sector would be unchanged. On the other hand, if the plates were at a higher or lower potential than the median plane, the focal distances would be shorter or longer, respectively. In addition to changing the focal lengths of the electric sector (condenser), the Matsuda plates also provide partial vertical focusing.

To improve the transmission of the mass spectrometer, a vertical focusing einzel lens, consisting essentially of three rectangular aperture electrodes, was placed between the electric condenser and the magnetic sector. The two outer electrodes of this lens were kept at the full secondary accelerating voltage potential. The potential of the center electrode could be varied in 20 steps from ground potential to the full acceleration voltage. This decel-accel einzel lens could be adjusted to provide a sufficiently short image distance for the entrance slit in the vertical direction so that the secondary ion beam did not strike the upper and lower pole pieces of the sector magnet. A short shield electrode was used to separate the entrance element of this einzel lens (at ground potential) from the electric field shunt electrode. The shield was kept at the same electric potential as the shunt electrodes.

The two shunt electrodes that were located at the entrance and exit boundaries of the electric condenser served to effectively terminate the cylindrical electric field described earlier in the discussion of fringing fields. These electrodes also acted to shield the incoming ion beam from the unsymmetrical electric field that would exist between the condenser and the angle slit, and also shield the outgoing ion beam from the unsymmetrical field that would exist between the condenser and the energy slit. Since the shunt plates were made of low carbon steel and were nickel plated (as were the other electrodes of the electric condenser assembly), they helped to shield the ion beam from the fringing field of the magnetic sector and any other stray magnetic fields. The shunt electrode potential could be varied between 76 and 100 percent of the full acceleration voltage by a 10 turn potentiometer.

The electric sector field or electric condenser, as it is often called, forced the ions into a circular path. The inner cylindrical condenser electrode was operated at the full negative secondary acceleration voltage while the outer cylindrical electrode was maintained at a less

negative potential. The ratio of the potential difference between these two electrodes to the full accelerating voltage can be calculated by assuming the equality of the centrifugal and electrostatic forces:

$$\frac{m v^2}{a_e} = \frac{e V_d}{d} \tag{25}$$

since

$$v^2 = \frac{2 e V'}{m} \tag{26}$$

The result is

$$V_d/V' = 2d/a_e = 0.435 \tag{27}$$

where V_d = voltage difference between the electrodes

V' = volt energy of the incoming ion beam (initial energy plus acceleration field energy)

d = distance between the cylindrical electrodes = 0.80 cm

a_e = mean radius of the ion path = 3.67 cm

If the ion beam had the full secondary acceleration voltage V along its trajectory within the electric condenser, then

$$\frac{V_d}{V'} = \frac{V - V_c}{V} = 0.435$$

or

$$V_c = (1-0.435)\ V = 0.565\ V \tag{28}$$

In practice, the ion beam does not have the full secondary acceleration voltage V along its trajectory, but is decelerated due to the lower negative potential V_c on the outer electrode. This less energetic ion beam is thus more easily deflected by the electric field V_d/d and so the potential of the outer plate V_c must be made more negative. That is, in terms of the negative potential, V_c must be greater than 56.5 percent of V. The electrode voltage control unit provided a variation of the condenser (outer electrode) potential from about 50 to 90 percent of the full secondary acceleration voltage in five coarse steps with an overlapping fine control potentiometer.

Ion detectors: The magnetic electron multiplier used to detect positive ions on the high mass scale was a Bendix Model M-306 multiplier. This multiplier is 4 x 0.81 x 1.32 inches in size and has built in Alnico V magnets which furnish a magnetic field of 400 to 600 gauss perpendicular to the electric field between the field strip and the dynode strip. Because of this relatively strong field, the magnetic electron multiplier is not sensitive to stray, low level magnetic fields. The cathode is located at one end of the dynode strip and is made of tungsten. The particles being detected enter the multiplier through a 90 percent transparent etched nickel mesh grid connected to one end of the field strip and strike the cathode. Both the field strip and the dynode strip are made of glass having a very high resistance coating (of approximately 10^8 ohms) on the active surface. No special treatment has been given to the dynode surface to enhance secondary emission and thus the multiplier can be exposed to humid air at atmospheric pressure for an indefinite period without injury. The anode of this multiplier is made of stainless steel. Kel-F spacers are used to provide mechanical support and electric insulation.

The magnetic electron multiplier is sensitive to photons having wavelengths less than 1500Å, positive and negative ions, neutral particles, and electrons. This instrument has a flat response, high gain (up to 10^8), low power requirement (200 mW), lightweight (4-1/2 ounches), a high time resolution (rise time less than 5 nanoseconds) and a low dark current (1 picoampere). The multiplier anode current can be as high as 0.1 microampere. For linear response, the anode dc current should not exceed 1/10 of the dynode dc strip current. The operating pressure at the multiplier should be below 5×10^{-4} torr. When operating at maximum current, hydrocarbon gas pressure in excess of 10^{-8} torr may result in an accumulation of deposits on the dynode surface.

This multiplier functions on the principle that an electron starting at rest in a crossed electric and magnetic field will describe a simple cycloidal motion perpendicular to the magnetic field, where the dips in the cycloid are directed along the equipotential lines of the multiplier. The equipotential lines in this multiplier are directed forward and slightly downward so that an electron strikes the dynode surface before it can complete a full cycle. Since it has a certain amount of kinetic energy (represented by the difference between point of origin and impact), secondary electrons will be generated at each impact. Each secondary electron repeats the same type of motion, and a cascading action results. The number of intermediate stages (impacts) is determined by the magnitude of the input and output differential voltages. The usual practice is to adjust these voltages so that the gain is optimized. Typical gains for this multiplier for various dynode strip gradients are given in Figure 7. The general method of connecting the magnetic electron multiplier is shown in Figure 8, while Table II shows typical operating voltages for the various electrodes. The potential difference between the dynode strip and the field strip should be 300 volts at the input ends and the output

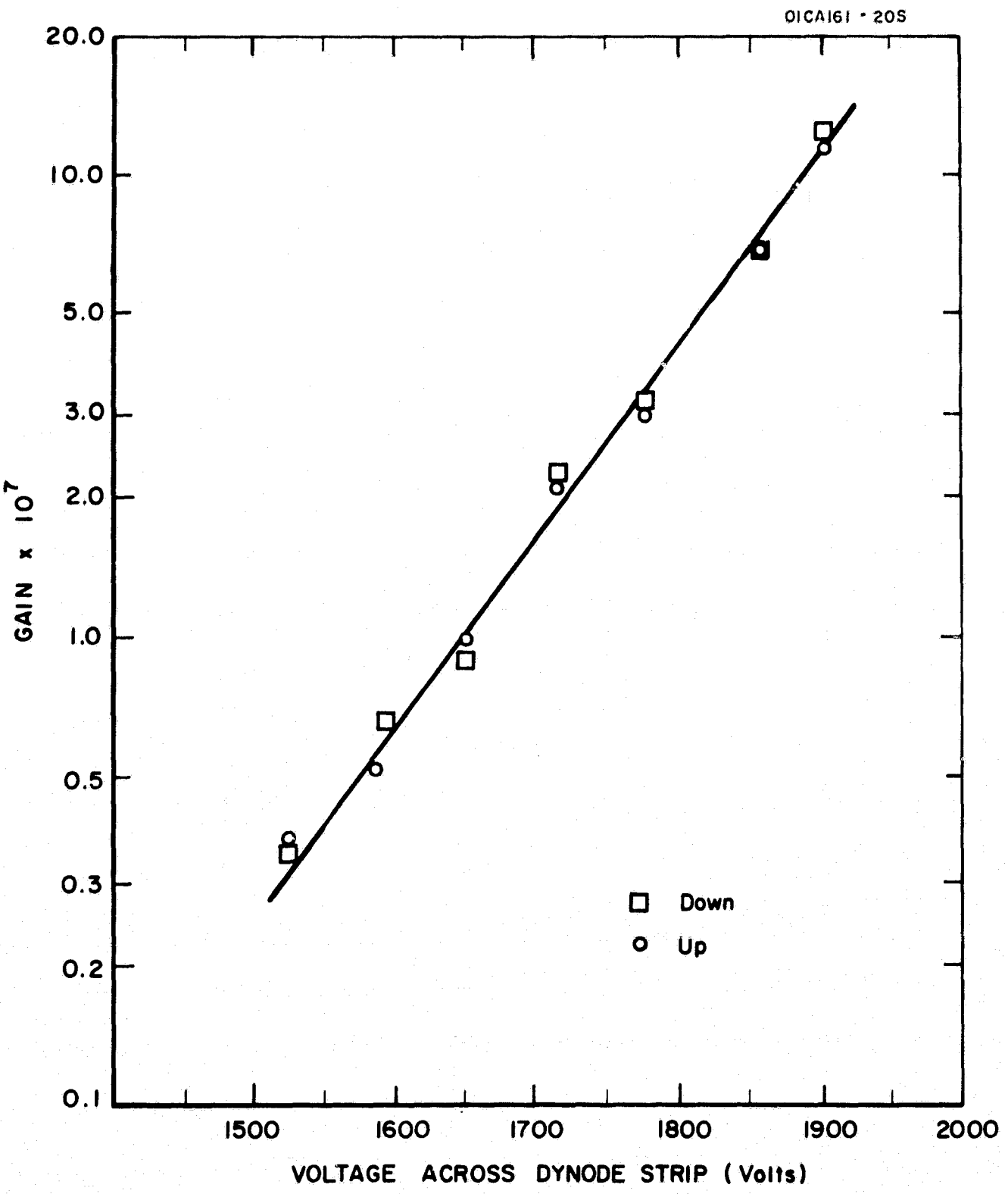

DSI (dynode strip input): varied FSI (field strip input): varied
DSO (dynode strip output): -62V FSO (field strip output): +192V
Potential difference between DSI and FSI = constant beta rays of Sr-90 used as constant input signal.

Figure 7. Typical gain of magnetic electron multiplier vs dynode strip gradient.

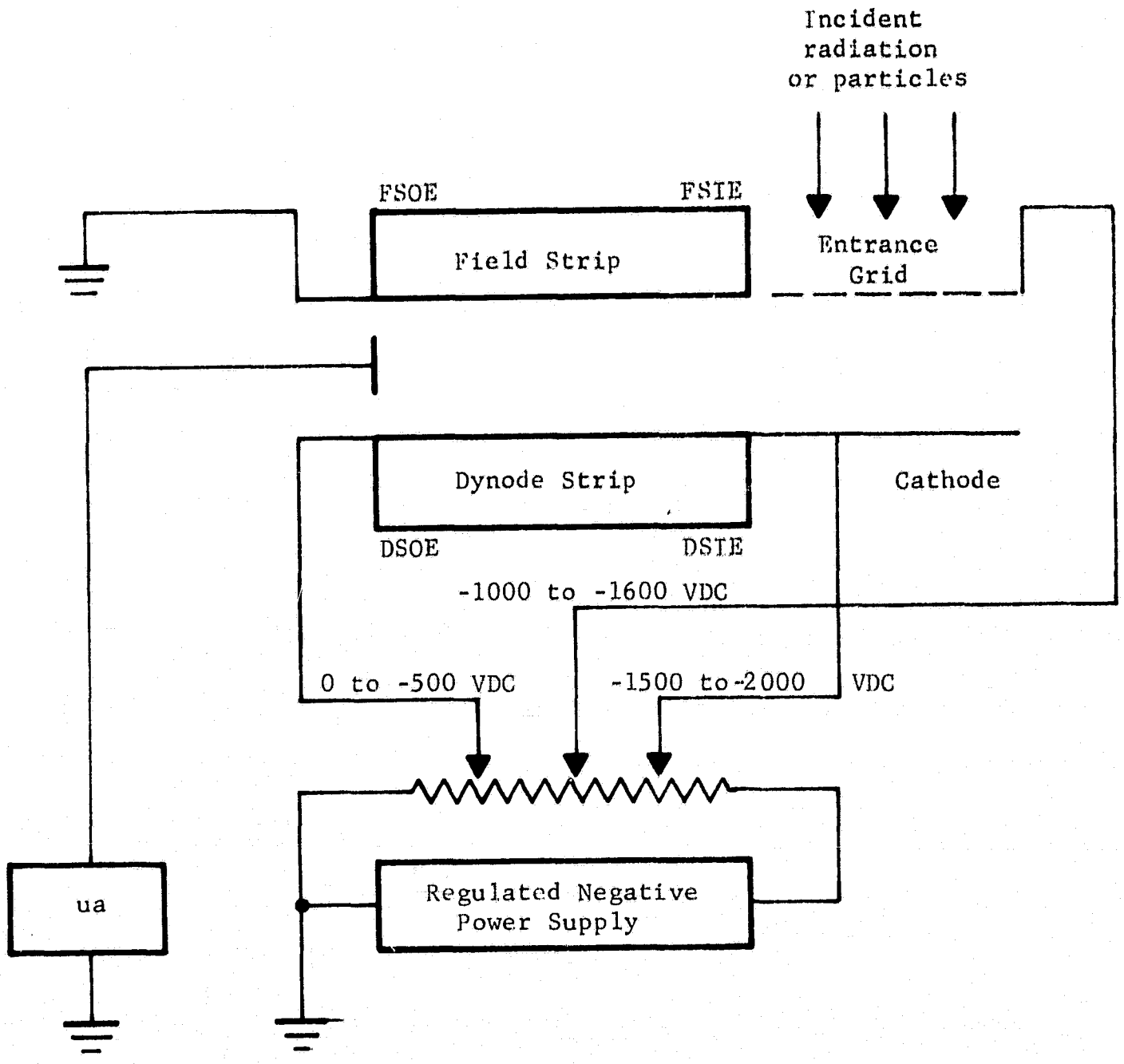

Figure 8. Schematic of magnetic electron multiplier showing typical electrical connections.

TABLE II

TYPICAL OPERATING VOLTAGES OF THE BENDIX M-306
MAGNETIC ELECTRON MULTIPLIER

Element	Normal Gain (volts)	High Gain (volts)	Low Gain (volts)
DSI	-1850	-2050	-1650
FSI	-1550	-1750	-1350
DSO	- 350	- 350	- 350
FSO	- 50	- 50	- 50

ends, with the field strip input and output ends being positive with respect to the dynode strip input and output ends.

Because of the rather large cathode of this multiplier, its position relative to the secondary ion beam was not critical. In addition, the focusing or defocusing action of the multiplier focusing plate was not critical.

The Channeltron electron multiplier used to detect positive ions on the low mass scale was a Bendix Model 4028 helix-shaped unit provided with an 8 mm diameter entrance cone. The helical shape of the multiplier subtended an arc of 840°. The channel i.d. was 0.040 inch while the channel o.d. was 0.080 inch. The radius of curvature of the helix was 0.24 inch.

The Model 4028 multiplier will respond to electrons, positive ions, negative ions, and photons within the spectral range from 1500 to 2Å. The gain of the multiplier is approximately 10^8 at a 3 kV operating voltage and the gain varies with voltage as shown in Figure 9. A recent multiplier of the Channeltron type, Model CRM 4010, is said to be sensitive to positive ions having energies of 2 keV and higher, and one should assume that this is true of all Channeltron type multipliers. Thus, for positive ions released at near zero potential, a negative potential greater than 2 kV is required at the multiplier input.

For the Model 4028 multiplier, the output current pulse width is 20 nanoseconds at a gain of 5×10^7. The average background current rate at a voltage of 3 kV is less than 4 counts/minute. The dynode surface resistance is 1×10^9 ohms. The maximum operating voltage is 4 kV, the maximum operating pressure is 1×10^{-4} torr, and the maximum dc anode current is 10 percent of the bias current for a linear analog response. This multiplier has a small size, light weight, low power consumption and a high electron gain.

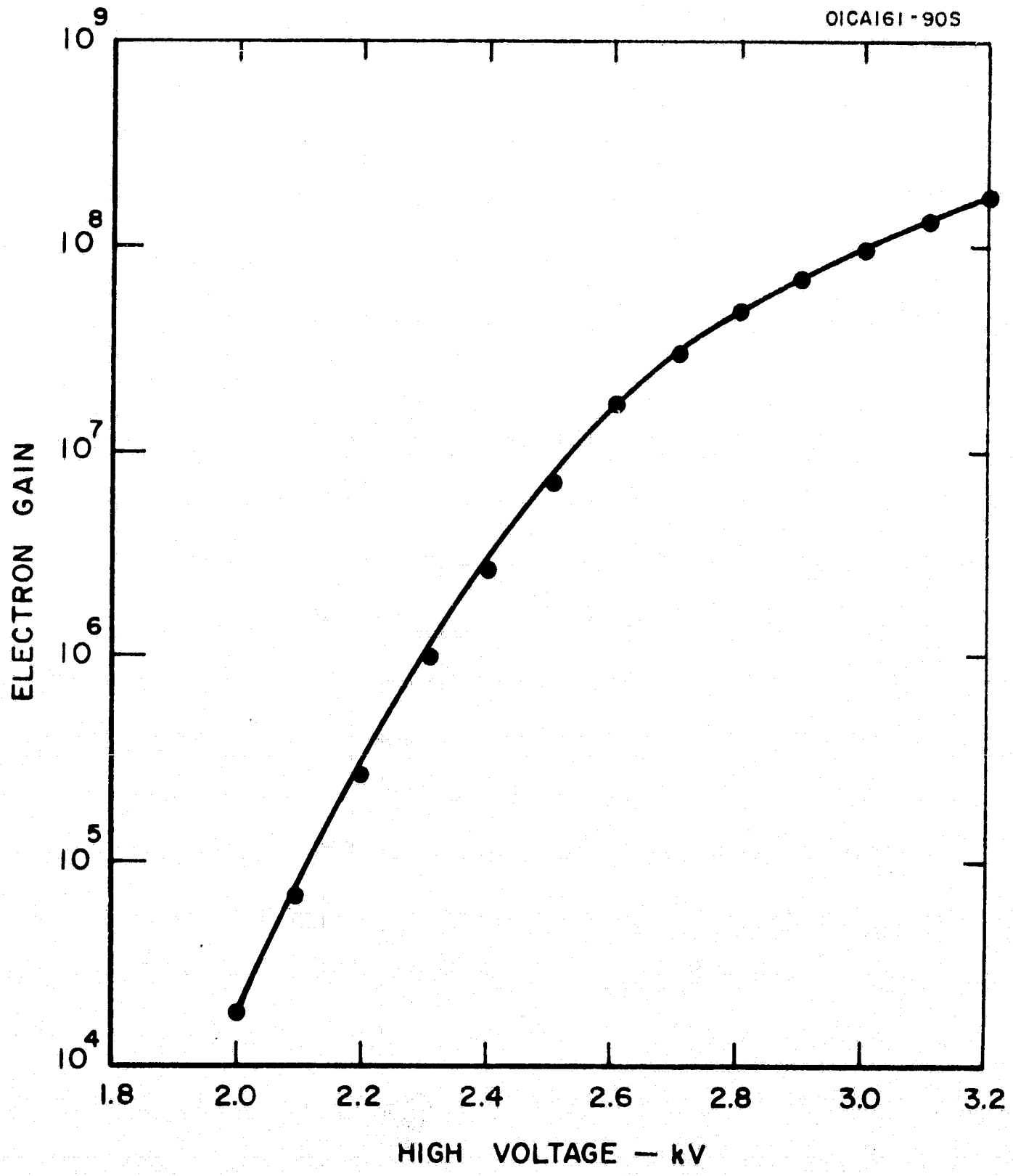

Figure 9. Typical gain of Channeltron electron multiplier as a function of voltage.

Basically, a Channeltron type multiplier is a hollow glass tube with its inside surface coated with a semiconducting material. The semiconductor surface serves as a secondary electron emitting dynode surface and also as a voltage divider which establishes the electrostatic field required to accelerate the secondary electrons.

A positive ion is detected when it enters the input aperture and impinges on the dynode surface. Electrons are emitted and are accelerated along the axis of the tube by the electrostatic field. Since the electrons have an initial velocity they also drift across the tube and strike the inner wall before they move very far in the axial direction. Upon collision with the wall, additional electrons are released and the process is repeated. The effective number of stages (collisions) and the gain per stage (ratio of the number of secondaries emitted per primary electron) finally result in an overall gain of the order of 10^8.

In applying the Channeltron multiplier to the detection of positive ions of the low mass scale, it was necessary to locate the multiplier quite close to the magnetic sector. The magnetic field at this location was relatively strong, and it is believed that this field had an adverse effect on the operation of the multiplier. It was also discovered that the positioning of the multiplier relative to the ion beam was critical. In order to improve the performance of the Channeltron, a grid was placed in front of the entrance cone and biased 300 volts negative with respect to the cone in order to keep secondary electrons emitted by the cone from being drawn to the exit slit (at the secondary acceleration voltage potential V). A small disc of metal about 2 mm in diameter and spaced about 1 to 2 mm from the output end of the Channeltron was used as an anode to collect the total electron current. The anode was connected through an electrometer to ground. The output end of the Channeltron was at a potential of 300 volts negative with respect to ground.

Power supplies and the control unit: Figure 10 is a detailed schematic of the complete electrical and electronic control circuitry used with the lunar lander mass spectrometer. The power supplies used to provide the positive and negative high voltages for the primary beam, secondary beam and electron multipliers were all John Fluke Model 408B well-regulated, digitally controlled output, dual polarity power supplies. These supplies could be adjusted for 0 to 6.0 kV output in discrete increments of 1, 10, 100 and 1000 volts. Load currents up to 20 mA could be drawn from these supplies. The power supply that was used to generate the mechanically swept, negative high voltage was modified by placing a linear 400 K ten turn potentiometer in series with the reference resistors R106 so that the voltage at the summing point would change as this resistance changed. A small 1 rpm motor was used to drive the 400 K potentiometer via pulleys and an O-ring drive belt. As can be seen from the schematic, the control unit consisted primarily of voltage divider circuits to supply voltages to the various electrodes.

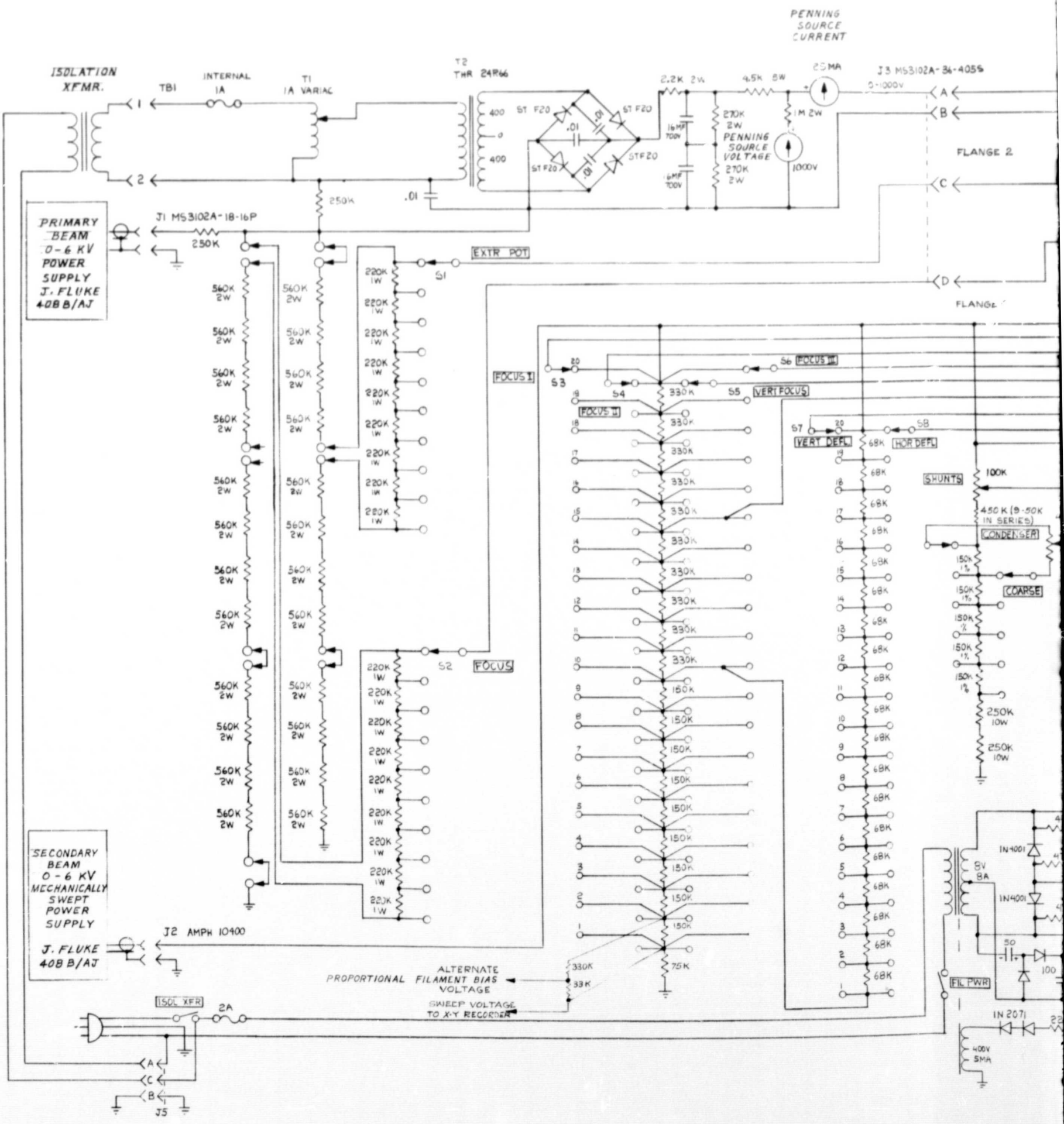

Figure 10. Lunar lander electrode volta

FOLDOUT FRAME 4

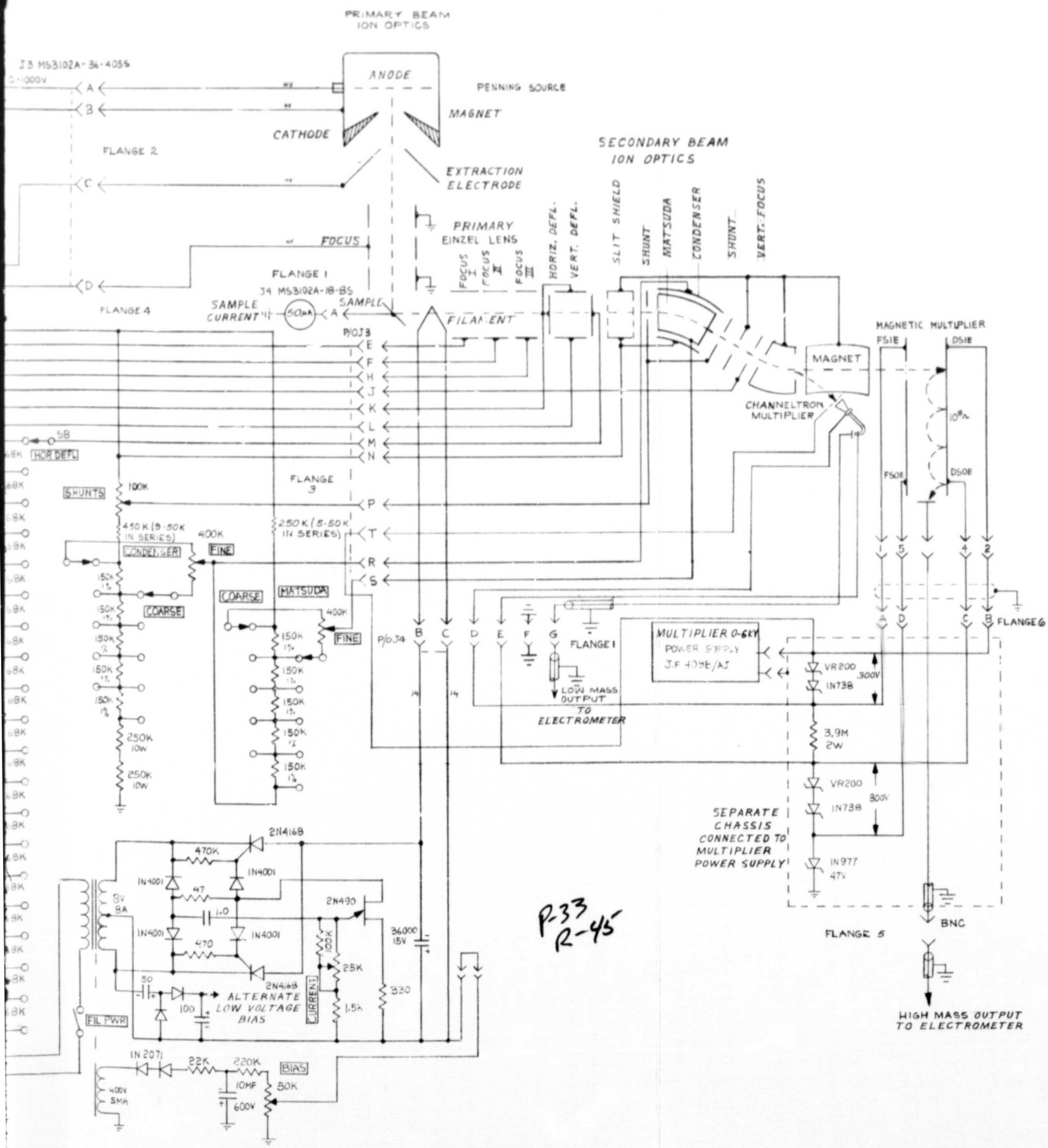

P-33
R-45

er electrode voltage control unit.

FOLDOUT FRAME
6

The Penning source supply, illustrated at the top of the schematic, used an isolation transformer to isolate the primary beam high voltage from the ac line. A small Variac autotransformer T1 was used to vary the ac voltage input to the Penning supply transformer T2. A full wave bridge rectifier followed by a filter section and a series dropping or stabilizing resistor of 4.5 K ohms furnished dc voltages up to +1000 volts to the Penning source anode with respect to the cathode. To provide better stability for this Penning source supply, the ac voltage input was sometimes obtained from the output of a line voltage regulator.

The cathode of the Penning source was connected directly to the primary beam positive high voltage. The separate voltage divider chains were used to provide voltages to the primary optics focus and extraction electrodes.

Four voltage divider chains, two of which were partially connected in parallel, were used to furnish voltages to the various secondary beam ion optics electrodes. These divider chains were connected to the negative 0 to 6 kV mechanically swept power supply as shown. The Matsuda voltage divider chain was connected to the condenser electrode voltage at its lower terminus so that the Matsuda voltage would always be greater than the condenser voltage, as required. In addition, small changes in the value of the condenser voltage would result in nearly proportionate changes in the Matsuda voltage.

The zener diodes used to establish the required 300 volt drops between the input ends of the field strip (FSIE) and the dynode strip (DSIE), as well as the output end of the field strip (FSOE) and the dynode strip (DSOE) were housed on a separate small chassis attached mechanically to the large high voltage output connector of the multiplier power supply. The same power supply was used to furnish the required voltages to both the magnetic electron multiplier and the Channeltron electrostatic multiplier. However, since the Channeltron normally operated with a voltage of 3.0 to 3.5 kV while the magnetic multiplier was operated at 1.6 kV, the two units were never operated simultaneously. When the Channeltron was being used during a scan of the low mass range, the multiplier voltage connections at flange 6 to the magnetic multiplier were disconnected by removing the octal plug at that flange. On the other hand, when the magnetic multiplier was being used during a scan of the high mass range, the Channeltron remained connected to the power supply, but its gain was too low to be effective. Additional circuitry could be provided to operate both multipliers simultaneously if the Channeltron unit is retained.

The charge neutralization filament power supply furnished filtered dc to the 12 mil diameter thoriated tungsten filament. The use of dc avoids the modulation of the secondary beam that could occur with an ac operated filament. A silicon controlled rectifier, fired by a unijunction transistor, regulated the filament power. The filament current was

adjusted by a phase shifting network which provided triggering of the unijunction transistor. The filament current could be adjusted between about 0 and 6 A. The maximum voltage under full load was about 10 volts. A separate toggle switch turned on the filament.

There were three separate sources of filament bias available in the control unit. The standard bias circuit could furnish up to approximately 175 volts of bias while the alternate low voltage bias circuit could furnish only about 16 volts of bias. In addition, an alternate proportional filament bias voltage was obtained from one of the regular voltage divider chains. The use of the proportional bias insured that there was no defocusing of the secondary ion beam as the secondary voltage was swept over its range.

A small fraction of the secondary sweep voltage was also provided to operate the X-axis of an X-Y recorder.

The electrode voltage control unit, the high voltage power supplies and the X-Y recorder were housed in a double electronic rack enclosure that could be moved around adjacent to the vacuum test system.

Vacuum Test System Design and Construction

The vacuum test system, as shown schematically in Figure 11 and in the photographs of Figures 12 and 13, was centered around the 24 inch diameter x 30 inch high steel bell jar test chamber. The circular base plate of the lunar lander mass spectrometer was mounted rigidly within a 5 inch high feedthrough collar that was positioned on top of the bell jar base plate and vacuum sealed by means of viton O-rings. This collar and the mass spectrometer base plate can be clearly seen in Figures 1 and 2.

The bell jar test chamber was pumped down by means of a 6 inch Edwards Model 6M3A mercury diffusion pump having an unbaffled speed of 600 to 650 liters/sec and an ultimate vacuum better than 5×10^{-7} torr when used with a liquid nitrogen cold trap. The bell jar was pumped through a 6 inch gate valve and a liquid nitrogen (LN_2) cold trap so that the effective speed of the diffusion pump at the test chamber was approximately 300 liters/sec.

The mercury diffusion pump was backed up by an Edwards 1SC 450D single stage mechanical vacuum pump having a displacement of 450 liters/min (15.75 cu ft/min). The mechanical pump was separated from the diffusion pump by a zeolite foreline trap that prevented backstreaming of mechanical pump oil into the diffusion pump and test chamber. Rubber hose connections were used between the mechanical pump and the zeolite trap and between the zeolite trap and the foreline.

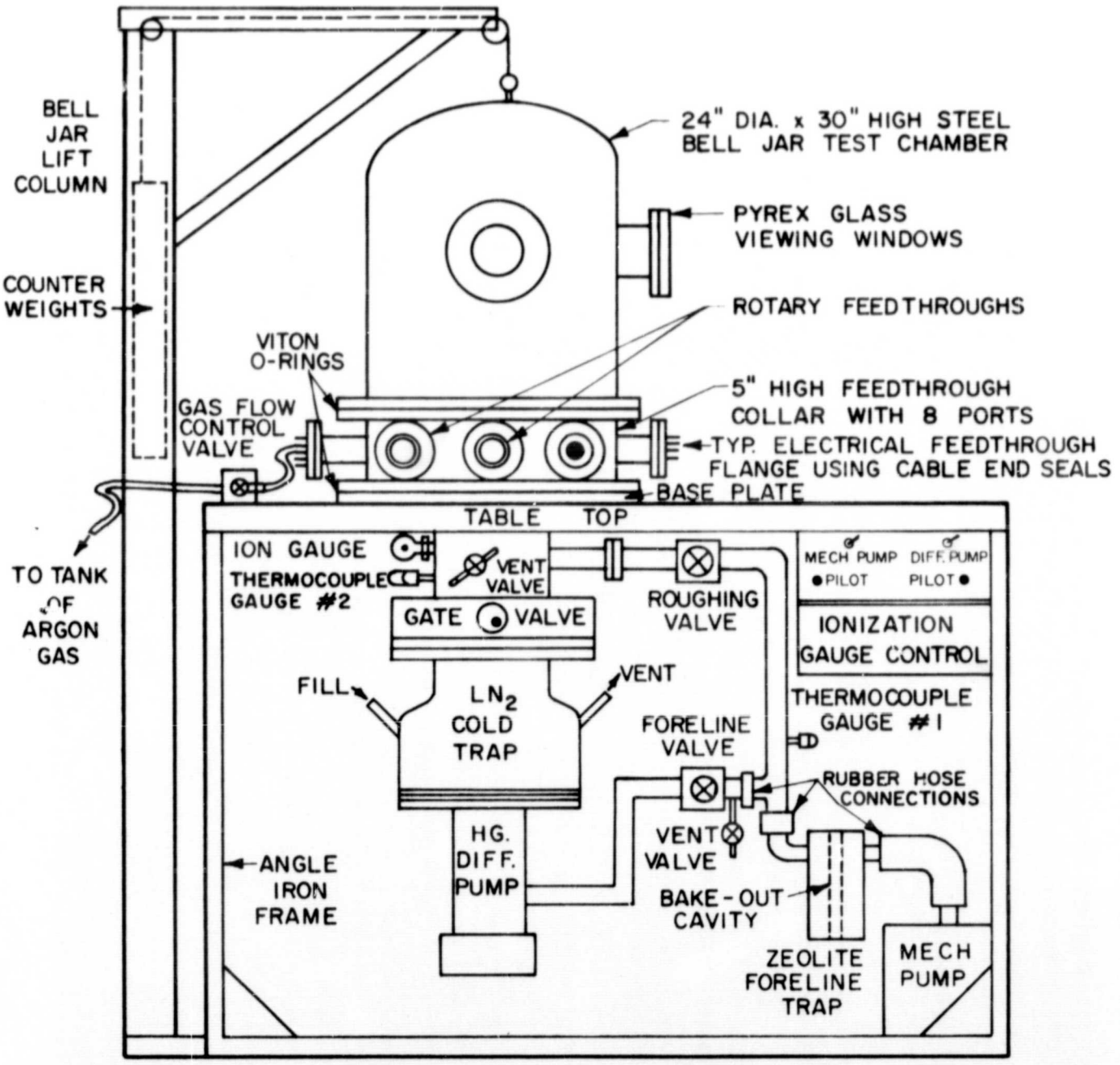

Figure 11. Schematic of vacuum test system.

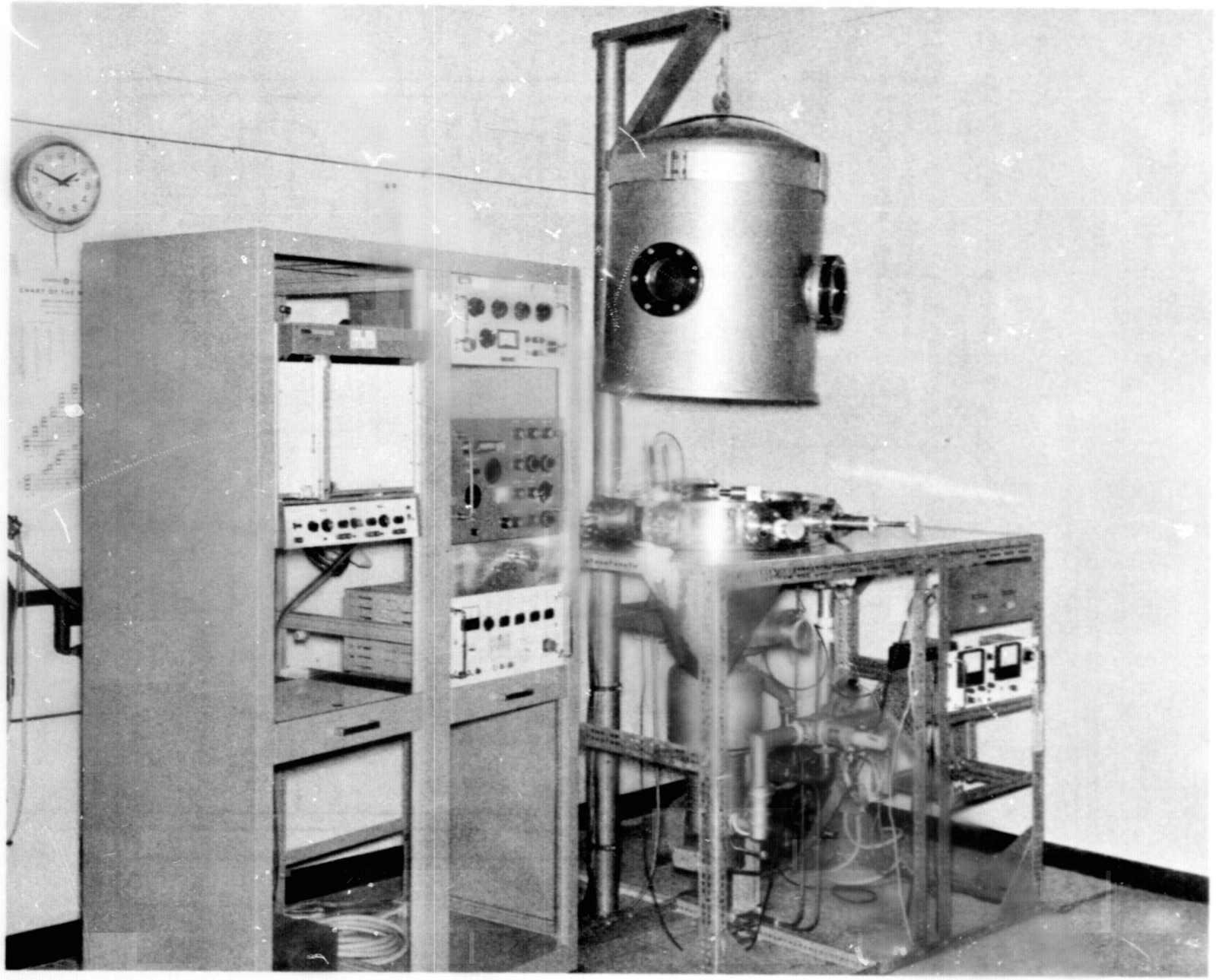

Figure 12. Photograph of vacuum test system with bell jar open.

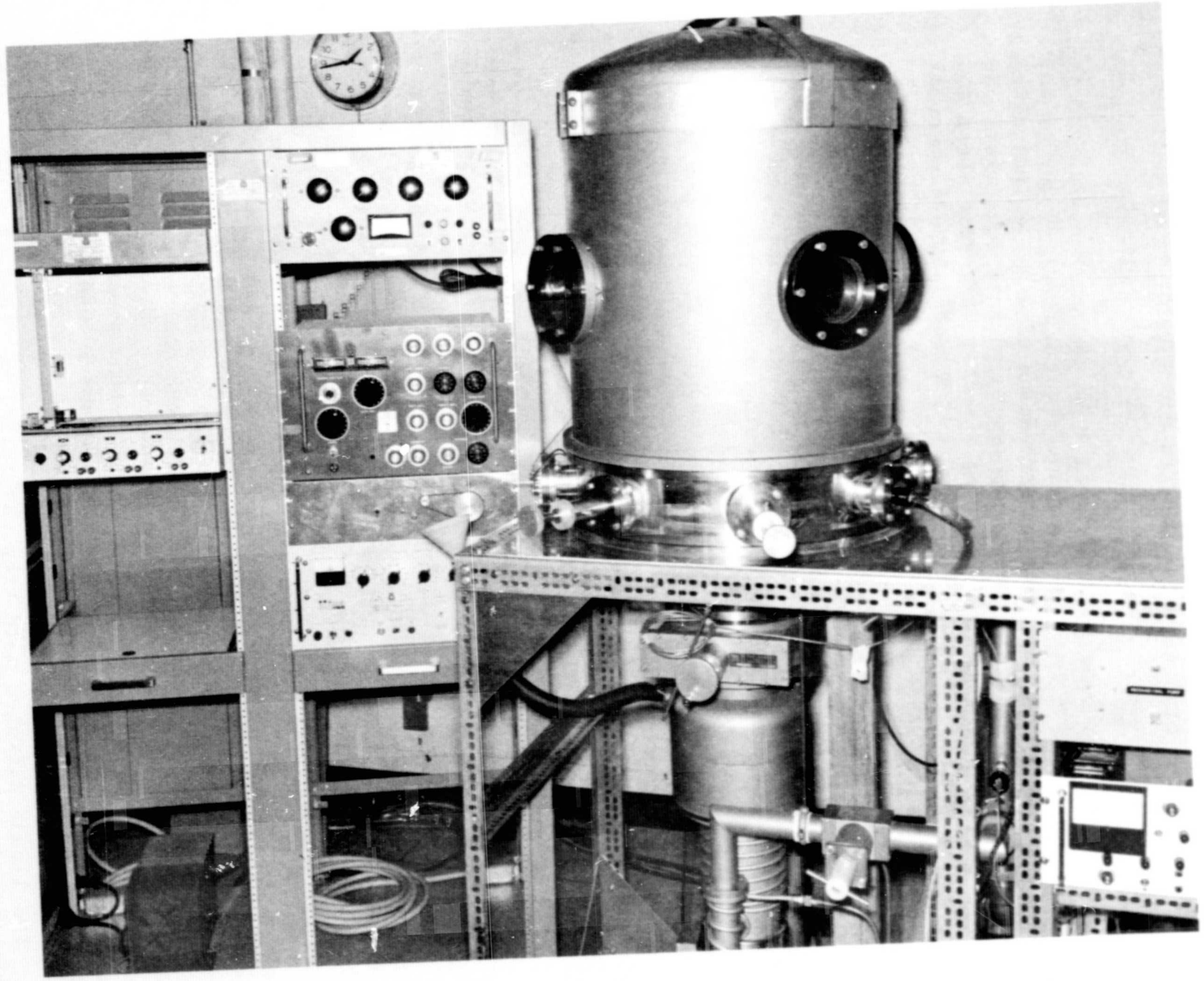

Figure 13. Photograph of vacuum test system with bell jar closed.

A foreline valve separated the diffusion pump from the mechanical pump and zeolite foreline trap while a roughing valve separated the test chamber from the mechanical pump and zeolite foreline trap. Both of these valves were 1-1/2 inch diameter Goddard Model VB19T brass bellows thru-flow type valves.

The liquid nitrogen cold trap was a Mt. Vernon Research Model 613 unit. The gate valve was a Mt. Vernon Research Model 61620-1-2 unit. The 5 inch high collar had eight ports sealed with 4-1/4 inch diameter flanges. These flanges had been modified to contain electrical cable end seal type feedthroughs, a 1/8 inch diameter stainless steel tube to carry the argon gas into the test chamber, an octal type electrical feed-through (glass insulated) and flexible shaft motion feedthroughs. Cylin-drical aluminum shields with transparent Lucite end plugs were provided to shield all the electrical feedthrough flanges.

The steel test chamber had three Pyrex glass viewing ports that used 6 inch diameter x 1/2 inch thick Pyrex glass sandwiched between the flange O-rings and flat outer gaskets. The viewing ports were used to illuminate the mass spectrometer, read the micrometers of the positioning stages, watch the primary beam, especially when focusing it with the help of a fluorescent screen, and watch for voltage breakdown and arcing between electrodes. A counterbalanced arrangement was utilized to facilitate raising and lowering of the bell jar. The bell jar flange would occa-sionally be clamped to the upper flange of the collar with C-clamps to speed up the rough pumping phase of the pump-down cycle.

A small Whitey 316 stainless steel Model 22RS2 needle valve with a micrometer stem adjustment was used as a flow control valve to admit argon gas to the Penning source. A Hoke Model 411 all-metal valve was soldered to the foreline between the foreline valve and the zeoline fore-line trap to act as a venting and leak-testing valve. A small brass O-ring sealed valve was fastened to the high vacuum tubulation above the gate valve to provide venting for the bell jar with the gate valve closed.

Three pressure gauges were used to measure the pressure in the sys-tem. A hot filament Bayard Alpert type gauge, a Vacuum Industries Model BA100K, of the nonburnout variety was installed via a quick coupling at the high vacuum tubulation above the gate valve. This gauge and two Hastings Model DV 6-M thermocouple gauges were controlled by a Vacuum Industries Model 9023 ionization gauge control. Thermocouple gauge #1 was located in the foreline to read the foreline pressure while thermo-couple gauge #2 was located at the high vacuum tubulation above the gate valve to read the test chamber pressure.

The liquid nitrogen cold trap was filled by means of a foam rubber insulated 3/8 inch diameter copper tube. A small plastic funnel was used to pour liquid nitrogen into the filling tube and cold trap from a 5 liter hand-held dewar. Cooling water was brought to the diffusion pump and dis-charged from it by 3/8 inch copper lines.

The supporting frame for the vacuum test system was assembled from drilled and slotted angle iron (Lyon Co. of Aurora, Illinois) reinforced with triangular gussets of 1/8 inch thick aluminum plate at each of the eight corners. A 3/16 inch thick aluminum plate formed the working table top of the system.

A separate power panel containing standard toggle switches to control the power to the mechanical vacuum pump and the mercury diffusion pump was mounted at the front of the frame. Two pilot lights were also mounted on this panel to indicate the "on" condition of the pumps. The ionization gauge control unit was mounted just below the power panel. All of the valves were accessible from the front of the supporting frame.

GENERAL SYSTEM TESTING AND OPERATION

The lunar lander mass spectrometer was put into operation using a step-by-step procedure. The first step or task was to obtain a low background pressure in the bell jar test chamber. The development and testing of the vacuum test system took several months.

The second step or task of the test plan was to establish the proper argon gas pressure in the Penning source of the primary ion beam system and then develop and test the primary ion beam optics.

The third task of the test program was to obtain a secondary ion beam from various sample materials and develop and test the secondary ion beam system. This was the most extensive portion of the test program.

The fourth and final task of the test program was to study the overall operation of the lunar lander mass spectrometer with a view toward improvement of its characteristics.

Mass Spectrometer Operational Characteristics

After the test system had been developed to the point where the bell jar pressure could be reduced into the low 10^{-6} torr region, testing of the mass spectrometer commenced.

The initial testing and operation of the lunar lander mass spectrometer consisted of establishing flows of argon gas through the Penning source, and operating the Penning source to get a primary ion beam. During the initial phases of operating the Penning source, it was found that the discharge within the source would start at a voltage of the order of 450 volts and a bell jar pressure of 5 to 6 x 10^{-6} torr. As testing continued, the required starting voltage increased to above 500 volts. A

gas pressure in the bell jar of about 6×10^{-6} torr corresponded to a Penning source pressure of about 10 microns, a value that was taken to be the upper pressure limit for continuous operation of the source.

When the Penning source was turned on and operated at a high source current of 25 mA or greater, the primary beam became visible in a darkened room environment. The beam could be seen directly as it came through the lower primary focusing electrode and struck the top surfaces of the sample holder and the focus I electrode. Reflected visible radiation from the beam also appeared between the extraction and focusing electrodes.

In order to focus the primary beam at the sample holder, a special fluorescent screen was prepared for installation at the sample holder. The screen was fabricated from a fine wire mesh (woven) stainless steel gauze that was impregnated with a slurry of Sylvania phosphor type CR-408 (aluminizing color) dispersed in a vehicle of Sylvania potassium silicate, electronic grade, type PS-6. Care was taken to avoid coating all of the wire surfaces, the ideal configuration being a disconnected series of phosphor squares filling the holes in the wire mesh. In this way, the primary ion beam would strike metallic wire surfaces and release secondary electrons to neutralize any positive charges that might tend to accumulate on the insulating phosphor surfaces. Such a phosphor screen would then be maintained at the same (ground) potential as the sample holder and would not charge up to the potential of the primary acceleration voltage.

The phosphor screen was installed by placing it horizontally on top of the sample holder so that the beam spot would be clearly visible over an extended area. It was reasoned that the small reduction in the object distance would have only a small effect on the focusing. The phosphor screen was connected electrically to the sample holder.

It was found that the primary beam tended to diminish in cross section and became brighter as the primary acceleration voltage was increased. By varying the divider chain (coarse adjustment) positions and the step switch positions of the primary focus and extraction electrodes, it was possible to either widen (defocus) or narrow (focus) the primary beam at the sample holder. A wide, fairly uniform primary beam was obtained with high values of positive extraction voltage (actually a minimum extraction field) and low values of positive focus voltage (a minimum focusing field). A broad beam with a bright central spot was obtained with a reasonable extraction potential (62 percent of maximum positive acceleration voltage at the extraction electrode) and a high focus potential of 94 percent of maximum positive acceleration potential. The smallest, brightest spot size at the sample holder was obtained with an extraction potential of the order of 30 percent of the primary acceleration voltage and a focus potential of the order of 86 percent of the primary acceleration voltage.

It was noticed that a glow discharge could develop in the tubing that furnished argon gas to the Penning source. The discharge developed when both the argon gas flow and the primary accelerating voltage were high. The occurrence of the discharge was inhibited by lengthening the tubing leading to the Penning source. A combination of bell jar pressures greater than 6×10^{-6} torr and primary accelerating voltages greater than 6.0 kV were avoided. With a bell jar pressure of 2×10^{-6} torr -- a nominal value that was frequently used -- the primary acceleration voltage could be increased to at least 8.0 kV without causing a glow discharge in the argon gas entrance tubing.

The argon gas pressure in the Penning source was over a thousand times greater than the equilibrium pressure in the bell jar. This meant that there was a substantial flow of neutral argon gas issuing from the Penning source and moving along the electrodes of the primary optics. Sharp points and edges of the primary optics lenses, or metal screws attached to the lens electrodes could cause corona discharges in the relatively high pressure argon gas environment when high voltages were applied to these electrodes. It was found that some of the metal screws holding the electrodes in position had to be replaced with nylon screws in order to avoid corona and arcing in the high pressure argon gas.

The location of the primary beam "spot" on the sample was adjusted by shifting the primary beam optics relative to the sample holder. Although the angle between the primary beam and the target surface normal could be varied, it was kept constant at 53.5° throughout the testing and operation phase of the program.

Whenever the Penning source was turned on, there was a momentary increase in the bell jar pressure of about 10 percent due to outgassing within the source. This pressure rise would subside after a few minutes of operation.

The primary beam spot size on the sample varied from a minimum of 1 x 1-1/2 mm for some samples to a maximum of 2 x 4 mm for other samples.

The use of a line voltage regulator to supply the 110 volt ac input to the Penning source power supply improved the stability of the Penning source. In general, it was found that the Penning source (discharge) current and the current to the sample (target current) were stable for source currents of about 1 mA or less and 10 mA or greater. The source was generally noisy and erratic for currents between 1 and 10 mA.

The current and power drawn from the primary beam acceleration voltage supply are listed in Table III. To this power requirement one must add the power taken by the Penning source supply as well as the power taken by the secondary electrodes, the electron multipliers and the neutralization filament.

TABLE III

PRIMARY BEAM ACCELERATION VOLTAGE, CURRENT AND POWER

Voltage (kV)	Current (mA)	Power (watts)
1.00	0.20	0.20
2.00	0.40	0.80
3.00	0.65	1.95
4.00	0.85	3.40
5.00	1.05	5.25
6.00	1.30	7.80
7.00	1.50	10.50

The initial testing and adjusting of the secondary ion beam system was performed with an aluminum sample since the sensitivity of a sputter source solids mass spectrometer is very high for aluminum. The secondary ion beam was first detected by collecting ions on the outer electrode of the cylindrical electric condenser. This electrode was connected through an electrometer (Keithley Model 600 battery operated unit) to the full secondary acceleration voltage. Since the inner electrode of the electric condenser was also at the full secondary acceleration voltage, the ion beam was not deflected by the condenser. No slit holders were used during the initial adjustment period so that only apertures of the order of 1/8 to 1/4 inch diameter limited the beam size.

It was found that both the sample (target) current and the current into the electric condenser increased as the primary beam voltage increased and as the secondary voltage increased, provided that the various electrodes were optimized. The horizontal and vertical deflection electrodes had a strong effect on the current collected by the condenser, as did the focus II and III electrodes. The shunt and Matsuda electrode potentials had only a small effect on the condenser current.

The different ways of optimizing the voltages on the focus II and III electrodes were evident. A relatively large condenser current signal was obtained with focus II at the full negative secondary accelerating potential and focus III at either a full negative accelerating potential or at zero potential. Also, a large condenser current was obtained with the focus II potential near zero and the focus III potential at its maximum value. The maximum current to the electric condenser with a primary voltage of 6.0 kV, a Penning source voltage of 500 volts, a Penning source current of 10 mA, a sample current of 44 microamperes, and a secondary acceleration voltage of -2.0 kV was 3.0×10^{-8} amperes, or slightly less than 0.1 percent of the target current.

Entrance and angle slit holders were then installed to limit the secondary beam size. The entrance slit holder had a 1/16 inch diameter aperture while the angle slit holder had a 1/8 inch diameter aperture. After adjusting the focus II and III electrode potentials (the vertical and horizontal deflection electrodes did not have to be changed), a maximum condenser current of 1.0×10^{-8} amperes was obtained, a value one third of that obtained without the entrance and angle apertures in position. With 0.010 inch wide slits used in the entrance and angle slit holders, the condenser current was further reduced.

In order to help adjust the secondary ion beam electrode potentials so that the beam passed through the electric condenser and into the magnetic analyzer, a special removable electrode was developed. This electrode was located within the aperture of the magnetic sector entrance shunt. It was connected electrically through an electrometer to the full secondary acceleration voltage (the same potential as the magnetic sector and its shunts). A nylon thread was attached to the electrode so that it could be pulled out of the way via one of the rotary feedthroughs (making use of its translational motion). When the secondary ion beam was finally detected at the magnetic electron multiplier, the removable electrode was no longer needed.

With the use of the removable electrode, it was found that the maximum secondary ion beam passed through the electric condenser when the potential of the condenser electrode (outer electrode) was about 65 percent of the secondary acceleration voltage. This setting was the most critical of all of the secondary electrode potentials. The second most critical setting was that of the horizontal deflection electrode.

The aluminum m/e 27 mass peak was first obtained at the magnetic electron multiplier without the detector slit holder in position. Initial optimum settings of the ion beam electrodes were measured and are presented in Table IV. The aluminum peak was rather broad and was surrounded by a high noise or scattered ion background. The dark current of the magnetic electron multiplier was quite high, having a value of about -5×10^{-10} amperes.

It was noticed rather early in the testing program that changes in the secondary accelerating voltage had a strong effect on the sample current and the primary beam. Making use of the fluorescent screen described earlier, it was determined that the primary beam "spot" was moved as much as 1/4 inch for a 500 volt change in the secondary acceleration voltage. This effect was practically eliminated by installing a cylindrical shield electrode between the lowest electrode of the primary beam einzel lens and the sample holder. The shield approached within 1/8 inch of the sample holder and was maintained at zero or ground potential.

Once the magnetic electron multiplier was effectively measuring the secondary ion beam signals, it was possible to make various measurements of the magnet and multiplier positioning. It was found that the best

TABLE IV

LUNAR LANDER MASS SPECTROMETER INITIAL OPTIMUM ELECTRODE VOLTAGE CONTROL SETTINGS

Control	Dial Setting	Percentage of Acceleration Voltage	Remarks
Primary focus	6	86	
Primary extraction	8	30	
Focus I	-	No connection	(Fixed voltage of -20 volts)
Focus II	17	21	
Focus III	20	21	
Vertical deflection	40	77.5	
Horizontal deflection	60	84	
Shunts	Full CCW	96.5	
Vertical focus	53	71.5	
Condenser coarse	3	64	(One 50K resistor of the bank of ten shorted out)
Condenser fine	070		
Matsuda coarse	88	78.5	
Matsuda fine	Full CW		
Multiplier			Magnetic multiplier voltage = -1600 volts

spectra (best resolution) were obtained with the multiplier axial position 3 mm away from its maximum outward position (setting of 90 on the scale). This corresponded to a distance of about 9.2 cm from the magnet to the exit slit, as compared to the theoretically calculated distance of 8.63 cm. The optimum magnet axial position was at 0.475 inch on the micrometer, placing the magnet at a position 7.2 cm relative to the energy slit, approximately equal to the theoretically calculated position.

The multiplier transverse position was varied and its effect on the m/e 27 aluminum peak was monitored. The optimum position for the multiplier was at a scale setting of 14.5 mm. The magnet transverse position was also varied from a micrometer reading of 0.790 to a reading of 0.670 inch. The location of the magnet in a transverse direction did not appear to be very critical over the region tested, but there was an optimum signal at a setting of 0.765 inch. The results obtained confirmed earlier measurements of the extent of the homogeneous magnetic field.

The magnetic electron multiplier dark current was initially found to change considerably from a low value of 1 or 2 x 10^{-13} ampere to a much higher value when the Penning source and various high voltages were turned on. For example, the dark current initially increased to about 1.5 x 10^{-10} ampere when the Penning source was turned on, and then decreased somewhat to 5.5 x 10^{-11} ampere when the +6.0 kV primary beam voltage was turned on. After shielding the multiplier with aluminum foil, the dark current with the Penning source on was reduced to 5 x 10^{-12} ampere, and the dark current with the +6.0 kV primary beam voltage on was 2 x 10^{-11} ampere, a definite improvement. The primary optics were shielded with a wire mesh screen and the multiplier and the magnetic sector were finally shielded with a single, large electrically grounded aluminum cover that permitted only the secondary ion beam to enter the magnet and multiplier region. After these shields were put in position, the multiplier dark current remained at 1 x 10^{-13} ampere even after the Penning source and the +6.0 kV voltage were turned on. Many other experiments had suggested that the high dark current was due to positive ions, electrons or metastable argon atoms produced in the Penning source. Because of the open structure of the developmental system, such energetic particles were undoubtedly moving throughout the test chamber. The paths of these particles and of secondary electrons released by them depended primarily on the primary and secondary acceleration voltages.

Not only was the multiplier dark current affected by the emission of energetic particles from the Penning source, but the background of mass spectra were exceedingly high for the same reason. For some of the early aluminum spectra, the background dc current level was about 2.5 x 10^{-9} amperes and the peak to peak ac noise was about 5 x 10^{-11} amperes. After complete shielding, the background current levels were as low as 1 x 10^{-13} amperes and the peak to peak noise levels were as low as 1 x 10^{-12} amperes.

The shielding of the magnetic analyzer and multiplier region reduced the stray ions and electrons that had previously masked the small secondary

beam mass peaks and, as a result, a multitude of new mass peaks became visible for the first time.

From time to time during the operation of the lunar lander mass spectrometer, the sample holder and adjacent electrodes were cleaned to remove the brown and black deposits that accumulated. It was assumed that these deposits were caused by the presence of hydrocarbons originating from the viton O-rings, the plastic tubing and other plastic materials within the bell jar. Cleaning was generally accomplished with either $A\ell_2O_3$ paper, $A\ell_2O_3$ powder within a nylon mesh (Beartex), or pure $A\ell_2O_3$ powder. Distilled water was used to rinse the surfaces after cleaning. The sides of the entrance slit holder and the angle slit holder facing the sample were also found to have deposits and were cleaned.

A listing of typical secondary beam electrode voltage control settings and the corresponding voltages (in terms of the percentage of the full secondary acceleration voltage) are listed for reference in Table V. The focus II and III settings and the horizontal and vertical deflection settings were invariable changed from one sample to another. Other controls such as the condenser, Matsuda, shunt and vertical focus controls were rarely changed.

A magnesium-aluminum alloy was installed in the sample holder and was used for a number of tests and experiments. The Mg-Aℓ spectra were relatively mass rich with mass peaks ranging from m/e 24 to m/e 90. These spectra permitted the first measurements of resolution to be made. Based on measurements made of peak spacing S and the peak width ΔS at half peak height for masses 25 and 26 (magnesium isotopes), the half width resolution was 76 according to the relationship

$$R = \frac{M}{\Delta M} = \frac{\Delta S}{S}\left(\frac{M_1 + M_2}{2}\right) \qquad (29)$$

On the same mass spectra, the mass 38 and 39 peaks could be seen to be fully resolved down to the baseline. All slits were 0.010 inch wide. On the basis of theory, the resolution of the mass spectrometer can be improved by reducing the slit widths.

The magnesium isotopes masses 24, 25 and 26 were clearly separated, but there was a high level background current since the mass analyzer and multiplier had not been completely shielded at the time. Perhaps for this reason, or perhaps due to interference from hydrocarbon peaks, the measured percentages of the 24, 25 and 26 peaks were 77.4, 11.9 and 10.7 instead of the accepted ratios of 78.70, 10.13 and 11.17.

Impurity masses such as sodium, silicon, oxygen, potassium, manganese, copper, zinc and zirconium were identified in the mass spectra. The copper and zinc isotopes were clearly separated, though not down to the baseline. The largest mass peak was the magnesium 24 peak with a

TABLE V

LUNAR LANDER MASS SPECTROMETER TYPICAL SECONDARY ION BEAM ELECTRODE VOLTAGE CONTROL SETTINGS

Control	Dial Setting	Percentage of Acceleration Voltage	Remarks
Focus I	4	2.8	
Focus II	40	46.5	
Focus III	40	42.0	
Vertical deflection	42	80.0	
Horizontal deflection	55	82.5	
Two common deflection plates	--	80.0	(This is a fixed connection)
Shunts	0	92.5	
Condenser coarse	3	65.0	(Range of 62.5 to 67.0%)
Condenser fine	560		
Matsuda coarse	88	83.0	(Range of 83.0 to 86.0%)
Matsuda fine	0		
Vertical focus	55	72.5	
Magnetic multiplier	--	----	-1600 volts
Filament current	85		(Filament glowing white)
Filament bias	--	2.8	(Connected to focus I potential)
Channeltron	--	----	-3000 volts

current of about 2×10^{-7} amperes at the output of the multiplier. Aluminum and magnesium oxides and hydroxides were present as they usually are for molecular spectra.

Magnesium-aluminum alloy spectra were taken with three different values of primary accelerating voltage, all other parameters remaining essentially unchanged. It was found that relative to spectra taken at 6.0 kV, spectra taken at 3.0 kV primary voltage had low mass peaks that were reduced by about a factor of five and high mass peaks that were completely eliminated. On the other hand, an increase in the primary beam voltage from 6.0 to 7.0 kV produced an increase in peak heights of only a few percent. This behavior was in general agreement with measurements of the sample and electric condenser currents as a function of primary accelerating voltage. The latter measurements were made with an aluminum sample and will be discussed in the next section.

The charge neutralization filament was operated primarily with dielectric samples, but on at least two occasions the filament was operated with metal samples to see if it had any effect on the mass spectra. No effect was noticeable. The filament setting of 73 on the dial would produce a dull glow at the filament. At this setting the filament voltage was 0.72 volts and the filament temperature was estimated to be 1400°K. A filament setting of 79 on the dial would produce a bright white filament having a voltage drop of 1.43 volts and an estimated filament temperature of 2000°K. The filament was generally operated at settings higher than 79 to provide large amounts of electrons. A good percentage of these electrons would flow up the positive ion beam and into the Penning source, where their presence would increase the Penning source voltage (less current would be drawn from the Penning source supply). The use of the filament allowed the argon gas flow to be reduced considerably and still maintain a discharge in the Penning source.

A low mass spectrum of magnesium-aluminum alloy was taken, using a 0.020 inch wide detector slit in front of the Channeltron electron multiplier.

A distinct mass peak appeared at a secondary voltage of 1600 volts, and this peak was tentatively identified as molecular hydrogen H_2, although hydrogen was expected at the much higher voltage of 2500 volts. Apparently the effective magnetic field strength over the trajectory of the low mass ions was much less than that over the trajectory of the high mass ions. This was undoubtedly the case since the low mass trajectory passed through a considerable length of the lower magnetic field that existed near the open edge of the magnet.

Another sample that yielded further information about the sensitivity and resolution of the lunar lander mass spectrometer was a sample of 321 stainless steel. On the high mass scale, mass peaks between m/e 23, sodium and m/e 125 appeared in the spectrum. The 58, 59 and 60 mass

peaks were resolved. Based on measurements of the silicon 29 and 30 mass peaks, the half width resolution was about 74.

The nominal amount of silicon in 321 stainless steel is one percent. Based on this percentage and on a minimum detectable signal of 8.5×10^{-12} amperes, the silicon 28 mass peak with an amplitude of 9.2×10^{-9} amperes indicated that one could detect 10 ppm by weight of silicon in 321 stainless steel. The nominal amount of chromium in 321 stainless steel is eighteen percent. Based on this percentage, the minimum detectable signal of 8.5×10^{-12} amperes and the chromium 52 mass peak amplitude of 1.7×10^{-8} amperes, the sensitivity of the mass spectrometer for chromium in 321 stainless steel was 90 ppm by weight.

Isotopes of iron, nickel, chromium, manganese, silicon, phosphorus and sulphur were identified in the mass spectrum. There was a large amount of sodium and potassium present initially, presumably as surface impurities. Oxides of iron, chromium and silicon were also present. The carbon peak was not seen because the secondary acceleration voltage could not be made large enough at the time the mass spectrum was taken.

One interesting characteristic of the stainless steel mass spectra was the presence of "memory peaks" carried over from earlier samples of magnesium-aluminum alloy and pure aluminum. The magnesium 24 and aluminum 27 mass peaks were especially strong, but magnesium oxide and aluminum oxide were also present. The memory peaks were observed to decrease with time.

Insulating or dielectric samples such as pure aluminum oxide and boron nitrude were tested next. The major peak in the aluminum oxide sample was aluminum 27, which had a large peak amplitude of 2×10^{-6} amperes. Since the minimum detectable signal was about 8×10^{-12} amperes, as little as 4 ppm of $A\ell_2O_3$ in a matrix of other minerals could be detected. Silicon and sodium were the two next largest peaks. Potassium and magnesium mass peaks were also present.

There was strong evidence that both the pure aluminum oxide and the boron nitride samples were charging up electrically even though the neutralization filament was used at many different current and bias settings. For example, the isotopic peak ratios of silicon in the $A\ell_2O_3$ sample varied from one mass spectrum to another. For the boron nitride sample, it was difficult to obtain two mass spectra that looked alike. Varying amounts of positive or negative charge on the surface of the sample would shift the mass spectrometer "energy window" relative to the ion energy distribution of each secondary ion species. The sample charge up varied with time and was manifested, in part by a time varying sample current. Sometimes all masses less than m/e 22 would be obliterated. At other times, masses as low as mass 11 (boron) would be clear and strong. The problem of insulating sample charge up will be discussed in a later section.

A copper-beryllium alloy sample was installed and tested on the low mass scale of the instrument. A broad beam of beryllium 9 was detected and the beam width was related to the wide aperture used in front of the Channeltron electron multiplier. The copper content of the sample was detected on the high mass scale, and the measured isotopic ratio of the 63 and 65 copper mass peaks was equal to the accepted value.

Since the copper beryllium alloy had only a small percentage of beryllium (of the order of 1 percent), a new sample of pure beryllium was installed. Mass spectra of the pure beryllium were taken on both the low and the high mass scales. The largest mass peak on the high mass scale was m/e 27 (combination of Aℓ and Be_3). Other mass peaks present were iron 56 and 54, BeO 25, BeOH 26, silicon 28 and 29, Be_2O 34, Be_2 18, potassium 39, argon 40, chromium 52, sodium 23 and magnesium 24.

On the low mass scale, using a 0.020 inch wide detector slit in front of the Channeltron multiplier, the beryllium 9 mass peak appeared for secondary acceleration voltages between 360 and 440 volts. The relatively small signal portion of the mass peak from 360 to 400 volts was identified with the "high energy tail" of the ion energy distribution. The peak from 400 to 440 volts had a maximum at 410 volts of 1.7×10^{-9} amperes (background current was 1.7×10^{-11} amperes).

The width of the beryllium ion beam could be determined roughly by the peak width. For example, for the 0.020 inch slit width used and the nominal ion trajectory radius of 2.00 inches, the percentage variation in radius was $(\Delta R/R) \times 100 = 1$ percent for an infinitely thin ion beam. However, the measured variation in the acceleration voltage was about ±20 volts for low energy ions only (400 to 440 volts), or a variation of about 5 percent. The measured incremental radius ΔR was equal to 5 percent of 2.00 inches or $\Delta R = 0.100$ inch. Thus, the effective beam width of the low energy beryllium ions was 0.100 - 0.020 = 0.080 inch. This relatively wide beam was caused by a number of factors including the absence of double focusing for the low mass scale, the inhomogeneity of the magnetic field near the magnet exit trajectory, the absence of an exit magnetic field shunt, the influence of the magnetic field on the Channeltron multiplier, and the difficulty of placing the detector slit within 1 cm of the magnetic field exit boundary, its theoretical location.

After the low mass scale was adjusted and "calibrated" for beryllium, the boron nitride sample was reinstalled with a platinum mesh screen (50 lines per inch) in front of the sample. It was hoped that the platinum screen would provide neutralizing secondary electrons that would prevent the boron nitride from charging up.

The mass spectrum taken on the high mass scale was relatively weak, presumably because of the "shadowing effect" of the platinum mesh screen. The largest mass peaks present were iron 56 and chromium 52, impurities in the platinum. There were also small amounts of silicon 28 and 29,

potassium 39 and 41, sodium 23, magnesium 24, aluminum 27, argon 40, oxygen 16, nitrogen 14, CH 13 and carbon 12 present.

On the low mass scale, the boron 11 and 10 peaks were separated but were resolved only down to 1/4 of the peak height. The ratio of the 11 peak to the 10 peak was somewhat less than two to one whereas the accepted ratio is four to one.

Vacuum Test System Performance

The vacuum test system worked pretty much as expected after all of the leaks were found and sealed. The nominal speed of the mercury diffusion pump of 600 to 650 liters/sec, unbaffled, was reduced to approximately 300 liters/sec by the intervening cold trap, gate valve and mass spectrometer mounting base plate. The approximate effective speed of 300 liters/sec was determined by measuring the pressure rise in the closed bell jar of known volume over a period of many hours, and then measuring the ultimate pressure in the bell jar after many hours of pumping. In both cases, the outgassing and permeation of gases through the O-rings of the system provided a relatively steady flow of residual gas. For example, a typical pressure rise of 2 microns per hour in the closed bell jar volume of about 266 liters was equivalent to a gas flow of about 1.5×10^{-4} torr liters/sec. The ultimate background pressure attained under these conditions was 5×10^{-7} torr, and thus the effective pumping speed was 300 liters/sec.

Pressure rise measurements in the closed bell jar generally yielded values between 1 and 3 microns per hour. Correspondingly, ultimate background pressures between 2.8×10^{-7} torr and 8×10^{-7} torr were generally attained after several hours of pumping. Typically, it took 3 to 4 hours of pumping to reduce the background pressure to 7×10^{-7} torr and 5 to 6 hours to attain a pressure of 3.5×10^{-7} torr.

A typical pump-down sequence was as follows: after the bell jar was closed, the roughing valve was opened to start the pump-down. During the period when the bell jar was opened for changing samples, etc., the mechanical roughing pump remained on and pumped the system up to the roughing and foreline valves. Usually the main gate valve and the foreline valve were closed and the mercury diffusion pump was under a partial vacuum. It took about 15 to 20 minutes for the pressure in the bell jar, as read by the TC-2 thermocouple gauge, to be reduced below 10 microns. The foreline valve would then be opened. The reading of the foreline pressure via TC-1 would give values that were approximately half of the bell jar pressure. With a foreline pressure of the order of 5 microns, the liquid nitrogen cold trap would be filled. It took about 10 liters of liquid nitrogen to cool down and fill the cold trap. The filling procedure was done by hand and took about 10 to 15 minutes. As soon as the cold trap was filled, the mercury diffusion pump would be turned on. Although

pumping action started in 20 to 30 minutes, the pump was allowed to operate about 1 hour before the main gate valve would be opened and the roughing valve closed. Approximately 5 to 10 minutes after the gate valve was opened, the hot filament ionization gauge was turned on, using its least sensitive range. The gauge was subsequently adjusted to follow the pressure decrease in the test chamber. By using this procedure, the gauge only operated in the 10^{-4} torr region for a short interval of time, thereby helping to keep it clean.

Temporary shut-down and venting of the bell jar was accomplished by turning off the diffusion pump, closing the main gate valve and turning off the ion gauge. The foreline valve remained open, the roughing valve remained closed, and the mechanical pump was kept running. The bell jar was vented to atmosphere by opening the vent valve on the test chamber tubulation and allowing atmospheric air to enter. After the liquid nitrogen in the cold trap had boiled off and the trap had warmed up to room temperature, the foreline valve was closed to isolate the diffusion pump and keep it under a partial vacuum. Water flow to the diffusion pump was never interrupted since cooling of the pump walls effectively minimized condensation of mercury at other points.

During the operation of the test system, several interesting characteristics of the system components came to light. For example, the construction of the diffusion pump boiler was such that not all of the mercury was removed from the pump when the drain line was opened. In fact, 3.15 pounds of mercury, more than half the total charge of 5.95 pounds, remained in the boiler. Over a period of many months of pumping, some mercury condensed into droplets on surfaces within the main gate valve and the cold trap. The presence of this mercury with its vapor pressure of about 1×10^{-3} torr increased the ultimate background pressure that could be attained in the system. If droplets deposited in or near the ion gauge tubulation, the ion gauge readings were unusually high. After very long exposure to mercury vapor, the ion gauge tube would be affected. The gauge tube filament emission became erratic and pressure readings would either oscillate or become erratic. Normal outgassing of the ion gauge tube did not remedy the situation and, eventually, a new ion gauge tube had to be installed. Liquid mercury never deposited in the test chamber. Mercury droplets in the gate valve and cold trap were removed by disassembling these units and cleaning them with acetone. New mercury was admitted to the diffusion pump on several occasions by removing the ion gauge and introducing a flexible teflon tube through the ion gauge quick coupling and down through the open gate valve and cold trap.

It was found that the liquid nitrogen cold trap would maintain some liquid nitrogen in its internal reservoir for over 3 hours, but it was best to fill it every 3 hours or even more often. About 5 liters of liquid nitrogen would be used up during each refill operation. When the cold trap reservoir was filled up, liquid nitrogen droplets rather than just the cold nitrogen vapor would emerge from the vent tube.

The gate valve was quite trouble-free. The only precaution that was taken with this unit was to avoid closing the valve too tightly. As the closure knob is rotated clockwise to close the valve, it moves very freely until the valve disc seats. When the valve disc seats, one can feel the resistance and it becomes more difficult to turn the knob. Closure of the valve is complete at this point, and further turning of the knob will not close the valve any tighter, but it can damage the valve.

The foreline and roughing valves did cause trouble during the system development period. Since these valves were opened and closed many times for testing purposes, the brass bellows of the valve stem would eventually crack. There is the possibility that mercury vapor affected the brass, but no positive signs of amalgamation were visible near the cracked portions of the bellows. After a while, these two valves were not opened fully in order to reduce the stressing of the bellows.

No leaks were ever found in any of the electrical feedthrough ports or flanges. However, leaks were found occasionally in the O-ring seal of the ion gauge quick coupling and in the viewing ports. The Pyrex glass viewing windows often cracked at the edges due to unequal stresses applied by the outer locking flanges. When these cracks became long enough in the radial direction, atmospheric air leaked through into the test chamber.

The foreline vent valve (the Hoke 411 valve) was soldered in position via one of its tubulations and thus it was not mounted as securely as it could be. This valve was always opened and closed by using two wrenches, holding the body of the valve with one wrench while the knob was turned with another wrench. Stresses on the soldered connection were minimized in this way.

It was found that the octal plug connections to the two thermocouple gauges would occasionally develop a poor electric contact. The poor contact would manifest itself by causing erratic or oscillatory readings of the gauge. The trouble was usually fixed by removing and connecting the octal plug several times to burnish the surface of the pins.

The zeolite foreline trap had to be baked out and reactivated after exposure to atmosphere. Bake-out was accomplished by inserting the rod heater into the central hole of the trap and plugging the heater into a 110 volt outlet. The roughing and foreline valves were closed and the mechanical pump was turned on with its vented exhaust in operation. The zeolite trap was generally baked for about 2 hours, and was then allowed to cool overnight. The progress of the bake-out and cool-down phases could be followed by watching the reading of the foreline thermocouple gauge TC-1. After the trap was at room temperature, the vented exhaust on the mechanical pump would be inactivated and the foreline pressure would decrease to its normal value of a few microns.

The motor used with the mechanical pump did not have a large enough starting torque to positively start the pump each time the mechanical pump switch was turned on. It was necessary to move the pump pulley by hand via the V-belt occasionally in order to set the pump in motion.

The rotary feedthroughs that were connected via flexible shafts to the magnetic sector mass analyzer and the magnetic electron multiplier worked very well. These feedthroughs transmitted translational motion as well as rotary motion through the vacuum wall. Because of the backlash in the flexible shafts, the amount of rotation imparted to the positioning stages had to be determined by watching the micrometer heads through one of the three viewing windows of the bell jar. A high intensity lamp was used to illuminate the positioning stages through a viewing window.

Occasionally, the base of the bell jar did not make perfect contact with the upper O-ring of the feedthrough collar at the beginning of a pump-down cycle. On these occasions, two large C-clamps were used at positions 180 degrees apart to draw the bell jar flange into contact with the O-ring. After the mechanical pump had reduced the pressure into the micron region, the C-clamps were removed.

The gas flow (argon gas was used exclusively during the developmental work) into the Penning source was regulated by the two stage tank regulator and the flow control needle valve. The tank regulator was adjusted to provide an output pressure of 1 to 2 psi (above atmospheric pressure). Flexible plastic (tygon) tubing connected the tank regulator output and the flow control needle valve. The needle valve had a micrometer drive stem that could be reset to any fixed position. The reproducibility of the valve setting with respect to the bell jar pressure was usually within 1/2 mil (0.0005 inch).

SPECIALIZED TESTS AND RESULTS

Source Efficiency Measurement and Calculation

The efficiency of the Penning source in the process of converting neutral argon gas molecules into argon ions can be determined by measuring and calculating the flow of neutral argon gas through the source, measuring the positive ion current to the sample and sample holder, and then finding the ratio of the ion current to the gas current.

The basic assumptions that were made in determining the source efficiency were:

(1) All neutral argon atoms enter the Penning source first and then flow through the exit aperture of the source (having a vacuum

conductance C) into the test chamber (bell jar) where they establish an equilibrium pressure above the background pressure due to a fixed effective pumping speed S of the diffusion pump.

(2) The argon atoms that are ionized in the source and which finally reach the sample and the sample holder are singly charged.

(3) There are no impurity ions.

(4) Secondary electrons and positive ions emitted by the target and target holder are negligible compared to the number of incoming positive ions of the primary beam.

The conductance C of the exit aperture of the Penning source was computed to be 0.26 liters/sec for argon gas from the equations below:

$$C = K' C_{orifice} \tag{30}$$

K' = Clausing's factor $\cong$ 0.65 for ℓ/a = 0.050/0.045 inches

where ℓ is the orifice length and "a" is the orifice radius.

$$C_{orifice} = 11.7\ A \text{ for nitrogen at room temperature}$$

$$11.7\ A\ \sqrt{M_{N2}/M_A} \text{ for argon at room temperature} \tag{31}$$

$$9.80\ A \text{ liters/sec for argon at room temperature}$$

where A is the cross sectional area of the orifice in cm^2.

$$A = \frac{\pi D^2}{4} = (0.7854)(0.05226) = 0.04105\ cm^2$$

Finally, C = (0.65)(9.80)(0.04105) = 0.26 liters/sec for argon at room temperature.

The calculation above is for molecular flow through the orifice and should be valid as long as the mean free path of the argon atoms is greater than the orifice diameter. Since the orifice diameter was 0.23 cm, such a mean free path would correspond to a pressure of about 20 microns in the Penning source. The Penning source pressure was usually kept below 10 microns and thus the flow was molecular.

The pumping speed for argon gas was taken to be 300 liters/sec. This was neither an exact or measured value but only an estimate based on the pressure rise measurements described earlier.

Making use of the continuity equation and the first assumption listed above, the gas flow of argon $\dot{Q}$ through the Penning source was

$$\dot{Q} = P_c\ S = P_s\ C = 300\ P_c = 0.26\ P_s \text{ torr liters/sec} \qquad (32)$$

where P_c was the bell jar pressure increase due to the argon flow (i.e., the difference between the final equilibrium pressure and the background pressure with no argon flow), and P_s was the Penning source pressure resulting from the argon flow.

The source efficiency is calculated below for two particular measurements of test chamber pressure and sample (target) current I_T:

Test A: $P_c = (2.7 \times 10^{-6} - 0.5 \times 10^{-6})$ torr $= 2.2 \times 10^{-6}$ torr

$I_T = 2.4 \times 10^{-5}$ ampere

thus $\dot{Q} = 300\ (2.2 \times 10^{-6}) = 6.6 \times 10^{-4}$ torr liter/sec

$= 6.6 \times 10^{-4}$ torr liter/sec $\times\ 3 \times 10^{19}$ atom/torr liter

$= 1.98 \times 10^{16}$ atom/sec

and $I_T = 2.4 \times 10^{-5}$ ampere $\times\ 6 \times 10^{18}$ ion/sec, ampere

$= 1.44 \times 10^{14}$ ion/sec

so that efficiency $= I_T/\dot{Q} \times 100 = 0.73$ percent.

Test B: $P_c = (3.6 \times 10^{-6} - 0.5 \times 10^{-6})$ torr $= 3.1 \times 10^{-6}$ torr

$I_T = 3.5 \times 10^{-5}$ ampere

then $\dot{Q} = 300\ (3.1 \times 10^{-6}) = 9.3 \times 10^{-4}$ torr liter/sec

$= 9.3 \times 10^{-4}$ torr liter/sec $\times\ 3 \times 10^{19}$ atom/torr liter

$= 2.79 \times 10^{16}$ atom/sec

and $I_T = 3.5 \times 10^{-5}$ ampere $\times\ 6 \times 10^{18}$ ion/sec, ampere

$= 2.10 \times 10^{14}$ ion/sec

so that efficiency $= I_T/\dot{Q} \times 100 = 0.75$ percent.

In both cases it can be seen that the source efficiency was low -- less than one percent of the atoms were converted into ions that reached the sample and sample holder. The low efficiency was partly a result of the low discharge current maintained in the Penning source. In Test A, the Penning source discharge current was 1 mA, while in test B the discharge current was 5 mA. The sample or target current also depended

strongly on the extraction and focusing properties of the primary beam optics as well as on the primary accelerating voltage.

Penning Source Voltage and Current Characteristics

The Penning source electrodes were connected to a variable dc potential (anode positive with respect to the cathode) through a ballast or regulating resistor. At a fixed gas pressure in the source, an increase in the potential or voltage across the source electrodes resulted in an increase in the source or discharge current. The voltage-current characteristic of the source over a limited range is shown in Figure 14. A very small change in gauge voltage gave rise to a relatively large change in gauge current over the region shown.

When the Penning source voltage was allowed to regulate itself via the ballast resistor and the argon gas pressure within the source was varied, the source current and voltage varied as shown in Figure 15. The discharge current varied approximately linearly with pressure over the current region from 1 to 10 mA and then began to saturate for higher currents and pressures. It appears that it would be advantageous to operate in the region of current saturation since the discharge current would be less affected by small changes in gas pressure and voltage. However, the stability of the source in this saturation region must be demonstrated positively. Operation at higher pressures caused a glow discharge to develop in the plastic tubing that delivered argon gas to the source, and, primarily for this reason, the source pressure was kept below 3 microns and the discharge current was kept below 1 mA for most of the tests. The Penning source was quite stable at the lower pressures and discharge current, but its efficiency was also low.

Sample Current Characteristics

The primary ion beam current that flowed to the sample and sample holder was a function of the ionization within the Penning source and the efficiency with which ions were extracted from the source and focused at the sample. Sample (target) current dependence on the discharge current within the Penning source is illustrated in Figure 16. There is a near linear relationship between these two currents as one might expect.

The relationship between the sample current I and the primary beam acceleration voltage V seemed to follow a power law (very close to a square law, $I = kV^2$) for voltages from zero to three kilovolts after which the current began to saturate with increasing voltage. It would appear from Figure 17 that not too much is gained in sensitivity for primary beam acceleration voltages greater than 4.0 kV.

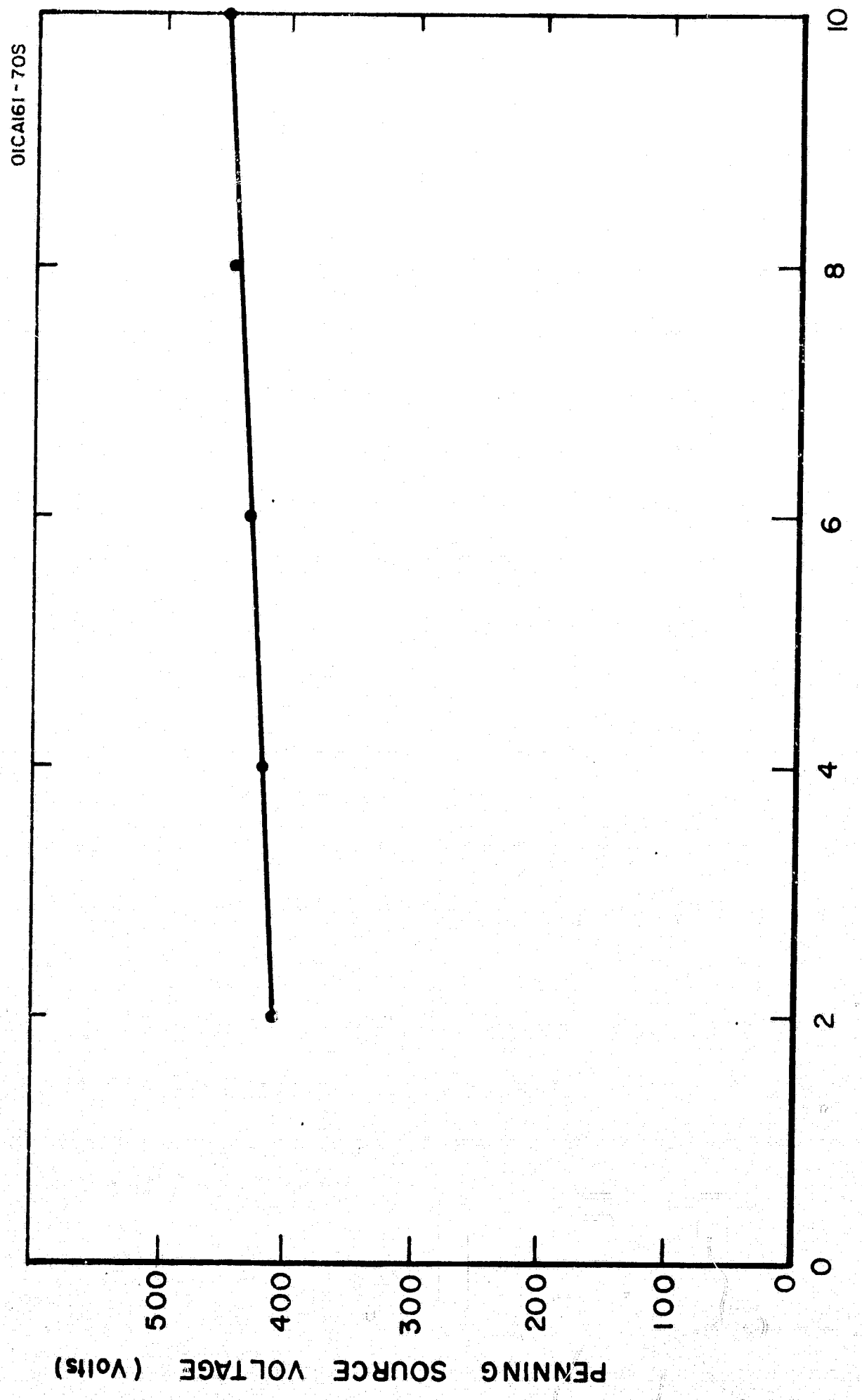

Figure 14. Voltage-current characteristic of the Penning source.

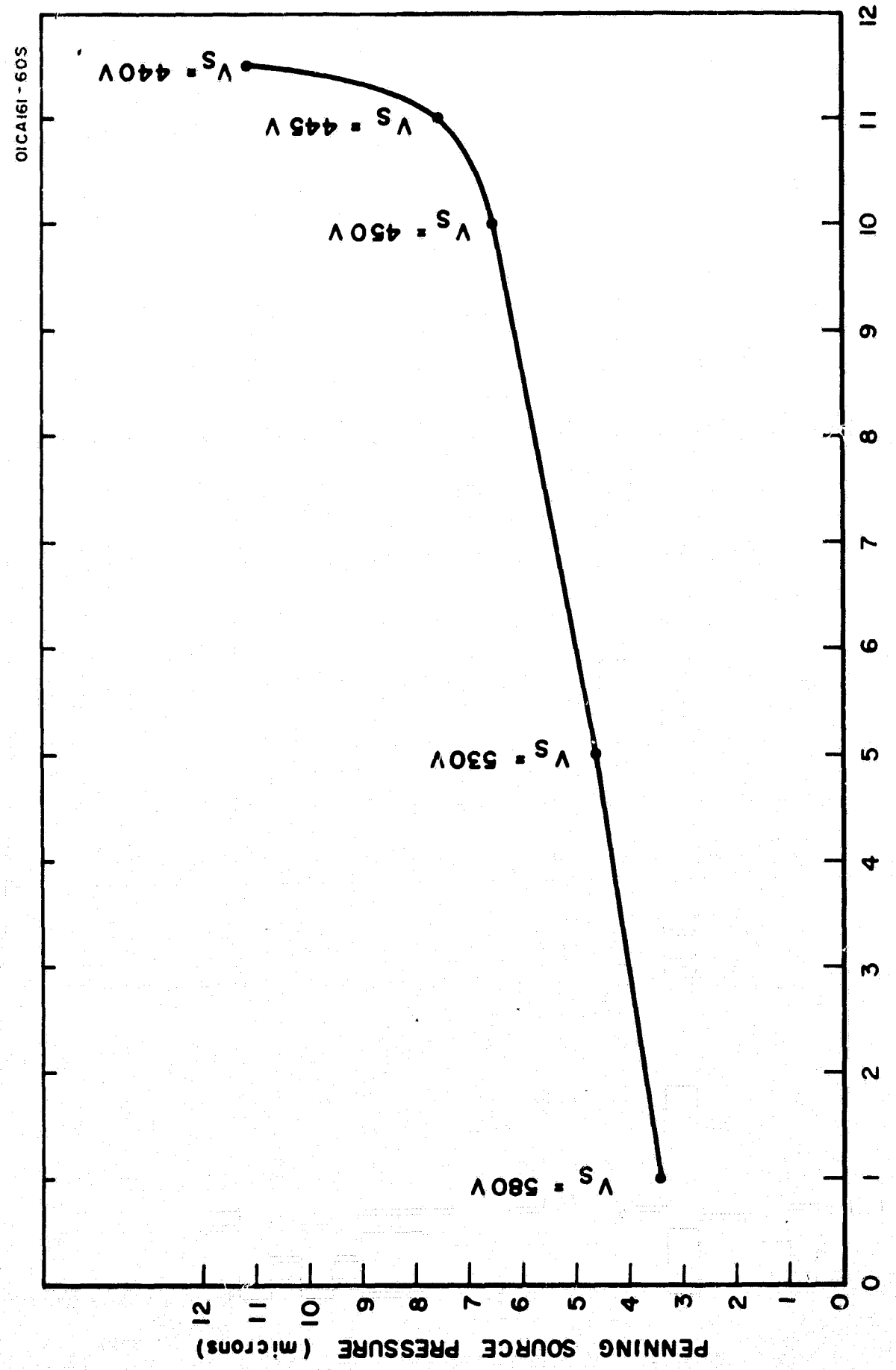

Figure 15. Penning source current and voltage vs. pressure.

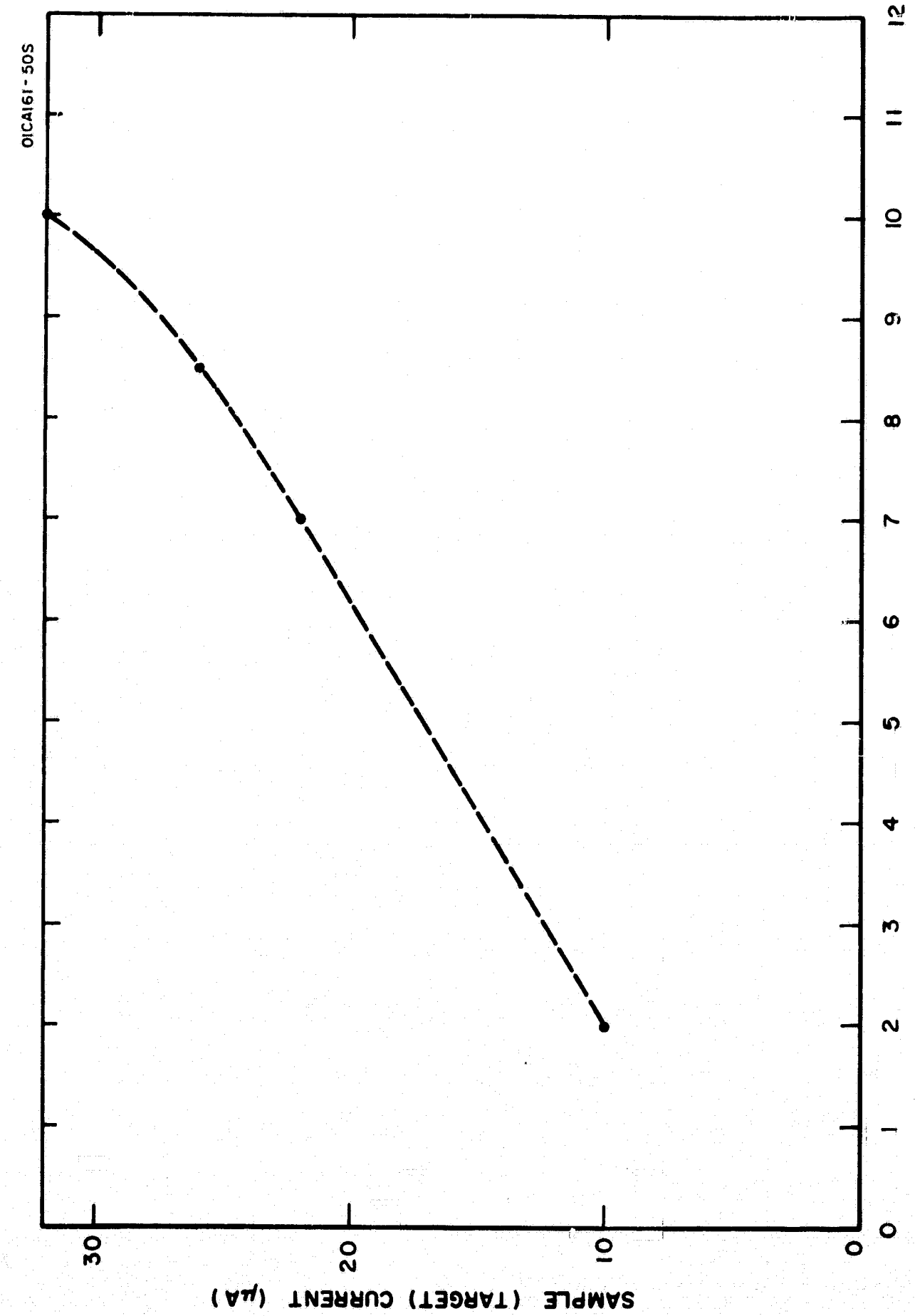

Figure 16. Sample current vs. Penning source current.

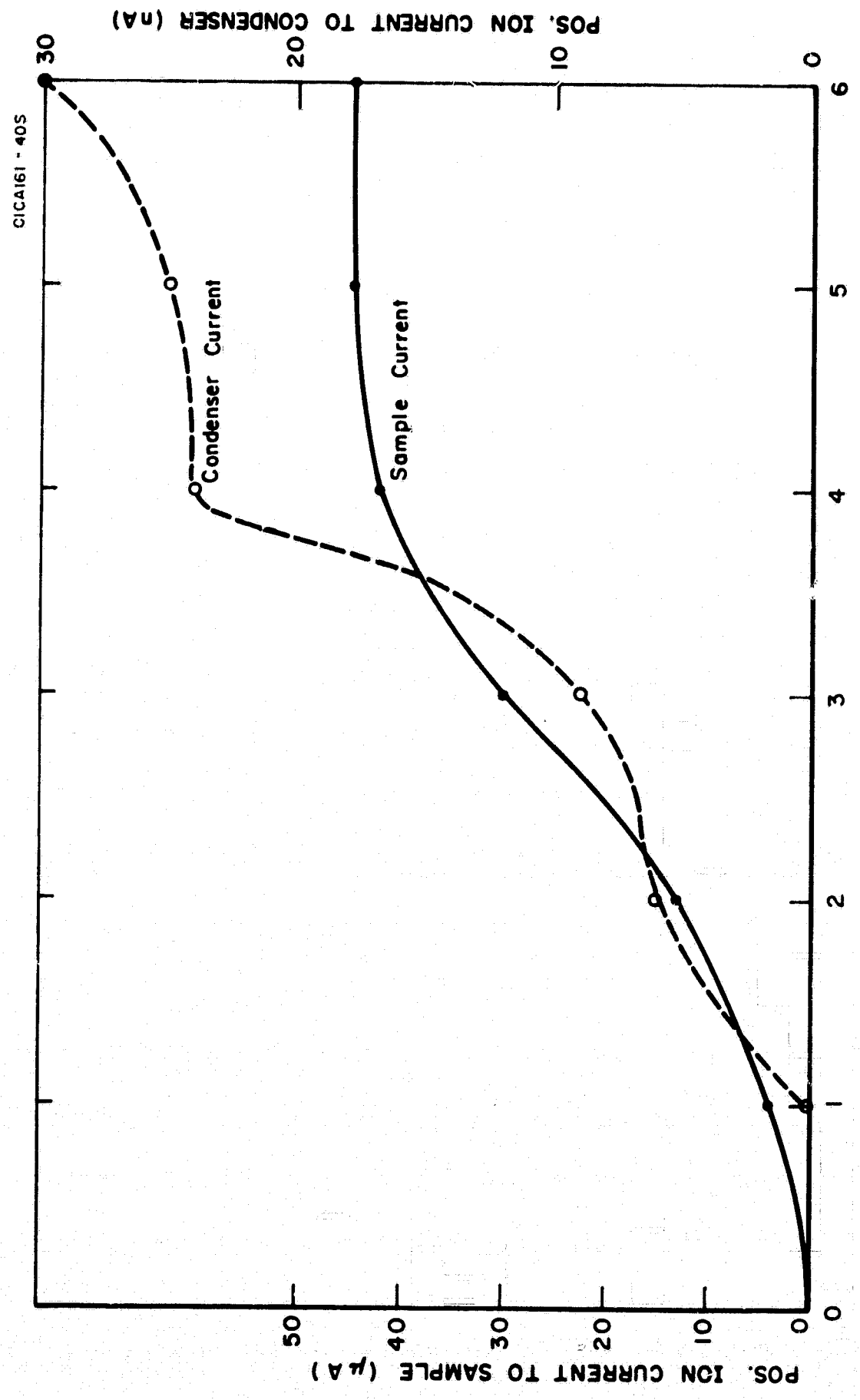

Figure 17. Sample and condenser currents as a function of primary beam acceleration voltage.

The sputtered secondary ion current (presumably mainly aluminum ions from the aluminum target) to the electric condenser varies in an unusual manner with respect to the primary acceleration voltage. Here again, however, there was a relatively large increase in current for acceleration voltages from zero to 4.0 kV and then a small increase above 4.0 kV. The ratio of condenser current to sample current did increase as the primary beam voltage increased above approximately 4.0 kV.

Achievement of a Linear Mass Scale

The basic operating equation of the mass spectrometer requires that the mass m of a molecule or atom being detected be inversely proportional to the secondary acceleration voltage V:

$$m = K/V \tag{33}$$

In addition, when the 10 turn potentiometer that controlled the accelerating voltage was moved at a constant speed, it was found experimentally that the accelerating voltage varied with time as shown below for increasing and decreasing voltages:

$$V_{INCR} = \frac{b}{c-t} \tag{34}$$

where b and c were constants such that $b/c = V_{MIN}$ at time $t = 0$.

Similarly, for a decreasing voltage, the relationship was

$$V_{DECR} = \frac{b}{d+t} \tag{35}$$

where b and d were constants such that $b/d = V_{MAX}$ at time $t = 0$.

Combining the equations above, it can be seen that the mass scale was directly proportional to the time for both increasing and decreasing acceleration voltages:

$$\begin{aligned} m &= (K/b)(c-t) \text{ increasing voltage} \\ m &= (K/b)(d+t) \text{ decreasing voltage} \end{aligned} \tag{36}$$

Mass Peak Amplitude as a Function of Sweep Speed

A test was made to determine the effect of sweeping over the high mass scale at two different speeds. The sample that was used for the test was the magnesium-aluminum alloy described earlier. All settings of the mass spectrometer were optimized to yield a maximum magnesium 24 mass peak having an amplitude of 2.5×10^{-7} amperes.

The Moseley Autograf Model 2FRA X-Y recorder was used to provide a pure time base X-coordinate sweep of 10 seconds/inch. The secondary beam accelerating voltage was varied in the usual manner with a 1 rpm motor driving a 10 turn potentiometer via a belt and pulley arrangement that changed the output voltage of a J. Fluke power supply. As shown in the preceding section, the spectrum mass varied linearly with time, and the amount of time taken to measure and record each mass was constant. The amount of time required to measure and record each mass peak was varied by changing the diameter of the motor pulley that drove the 10 turn potentiometer. In one case, the pulley diameter was kept at its usual value of 3/4 inch. In the second case, the pulley diameter was increased to about 1-5/8 inches, roughly twice its normal value. The increase in the pulley diameter approximately doubled the sweep speed.

The sweep speed test consisted of scanning a portion of the magnesium aluminum spectrum from mass 37 to mass 50 at the two different sweep speeds and recording the results. If no elements of the mass spectrometer detection and recording system limited the amplitude of the mass peaks, then both spectra would be identical except for the different peak widths. If, however, the speed of response of one or several elements of the system affected the peak amplitudes, this would cause a decrease in the peak amplitudes for the faster scan.

The results of the test are displayed in Table VI. It is evident that the amplitude of the mass peaks was being limited by one or several elements in the system, the most likely elements being the Keithley electrometer and the X-Y recorder. The potassium 39 mass peak may have decreased naturally between the time of the first slow scan mass spectrum and the later fast scan mass spectrum.

TABLE VI

COMPARISON OF PORTIONS OF MAGNESIUM-ALUMINUM ALLOY MASS SPECTRA TAKEN AT DIFFERENT SWEEP SPEEDS

Mass Number	Element	Peak Height (Fast Scan) 5 sec/mass peak	Peak Height (Slow Scan) 10 sec/mass peak	Percentage Increase
48	Mg_2	1.80 inches	2.00 inches	11.1
43	MgOH AℓO	1.20	1.40	16.7
42	MgO MgOH	1.60	1.85	15.6
39	K	1.35	1.70	26.0

Measurement of Isotope Ratios

A mass spectrometer is a unique instrument in that it can measure the isotopes of each basic element. This capability makes the mass spectrometer valuable in age determination analysis. The accuracy with which isotope ratios have been measured to date with the lunar lander instrument is given in Table VII.

One of the largest sources of error in measuring isotope ratios is the unsuspected presence of unknown interfering mass peaks. Such mass peaks are kept to a minimum by measuring relatively pure homogeneous samples of the elements under investigation. This was not done in the case of the isotopes listed in the table. Additional errors may be caused by memory and background effects. When the isotopes are widely separated in mass, the usual mass discrimination effects introduce errors.

Beryllium Mass Peak Instability

A test was made on the low mass scale to determine the stability of the beryllium 9 mass peak in a copper-beryllium alloy as a function of time. The controls were first adjusted to optimize the mass 9 peak. The center of the peak was then located and the accelerating voltage corresponding to the peak center was determined. The accelerating voltage was kept at the determined value for a period of almost 700 seconds while the electrometer output signal was recorded on the X-Y recorder. The target current was also monitored during this internal.

It was found that during a time internal of about 250 seconds, the beryllium 9 mass peak amplitude decreased from a maximum value of 4×10^{-10} amperes to a minimum value of 1×10^{-10} amperes. After this initial behavior, the signal increased and began a slow irregular oscillation about a value of 2×10^{-10} amperes. The target current varied between 4 and 5 microamperes during the total test interval. The gas pressure was constant.

The copper-beryllium alloy wire used in this test was wound into short horizontal segments and was backed up by an insulating sheet of aluminum oxide. The variations in the signal could have been caused by any one of the following effects:

(1) Charge-up of the backing aluminum oxide.
(2) Charge deflection of the primary beam.
(3) Charge deflection of the secondary beam.
(4) Channeltron multiplier instability.
(5) Variations in the alloy composition or homogeneity.

TABLE VII

MEASUREMENTS OF ISOTOPE RATIOS

Element	Mass Number	Measured Ratio	Accepted Ratio	Error
Magnesium in a Mg-Aℓ alloy	24	77.4%	78.70%	- 1.65%
	25	11.9	10.13	+17.5
	26	10.7	11.17	- 4.21
Silicon in a 321 stainless steel alloy	28	91.2	92.21	- 1.09
	29	5.7	4.70	+21.3
	30	3.1	3.09	+ 0.34
Chromium* in a 321 stainless steel alloy	52	93.1	95.11	- 2.11
	50	6.9	4.89	+41.1
Copper in a Cu-Be alloy	63	69.3	69.09	+ 0.30
	65	30.7	30.91	- 0.67

*The chromium 53 and 54 isotopes were omitted because of interference.

Evidence of Insulating Sample Charge-up and Filament Bias Tests

There were several indications that insulating samples were charging up and varying in potential. The tests made with boron nitride yielded many different mass spectra of the same sample. The ratios of various mass peaks changed considerably from one mass spectrum to another even though the electrode voltages remained unchanged.

Another manifestation of charge-up was shown by an aluminum oxide sample. The ratios of the isotopes of a silicon impurity in the sample changed drastically from one sample to another, and neither set of ratios was close to the accepted ratios.

Still another indication of charge-up of insulating samples was the erratic and wide variation of the sample current. The sample current could be changed with the use of the neutralization filament, but current variations persisted.

The neutralization filament was tried out with all of the insulating samples under a variety of conditions. The filament current, and thus the filament electron emission was varied over a wide range. The negative

filament bias with respect to the sample holder potential was made as large as 185 volts in an attempt to deliver electrons to the sample. In no case was there any indication or evidence that the sample charge was being neutralized.

TYPICAL MASS SPECTRA
(See Figures 18 through 24)

The mass spectra presented in this section will provide concrete information concerning the current capability of the lunar lander mass spectrometer. Since the electrometer that was used to amplify the output of the electron multipliers was a linear manually range switched unit, each mass spectrum was taken with only a single decade range of mass peak amplitudes. Thus, many of the spectra have saturated current peaks that are not measurable. Many mass spectra were taken at reduced electrometer sensitivity to record the amplitude of the largest mass peaks after the smaller peaks had been recorded. In some cases, such as for the magnesium-aluminum alloy mass spectrum, the electrometer range was switched during the scan. In this spectrum, mass peaks from sodium 23 through silicon 28 were taken with reduced electrometer sensitivity (10^{-9} ampere scale) while the higher mass peaks were taken with increased electrometer sensitivity (10^{-10} ampere scale). All of the atoms and molecules identified on the spectra were singly charged.

All of the spectra shown were taken with a primary argon ion beam of 6.0 keV energy. In each case, the equilibrium gas pressure in the test chamber was about 2×10^{-6} torr compared with a background pressure of about 5×10^{-7} torr with no argon gas flow. The Penning source voltage was about 750 volts and the discharge current was about 0.5 mA for each mass spectrum. Target currents in each case were of the order of 5 μA. The magnetic electron multiplier used for the high mass scale spectra was operated at -1600 volts while the Channeltron multiplier used for the low mass scale was operated at -2700 volts. The neutralization filament was off when the metal samples were analyzed and was on for the insulating samples.

DISCUSSION AND CONCLUSIONS

Summary

A small, miniaturized, double focusing solids analysis mass spectrometer was designed, constructed and tested. The solid sample being analyzed was bombarded by a high energy primary beam of argon positive ions. The primary beam was focused to irradiate the sample over a few square millimeters of area. Secondary ions created in the sample at and near the surface were drawn off and formed into a secondary ion beam. The

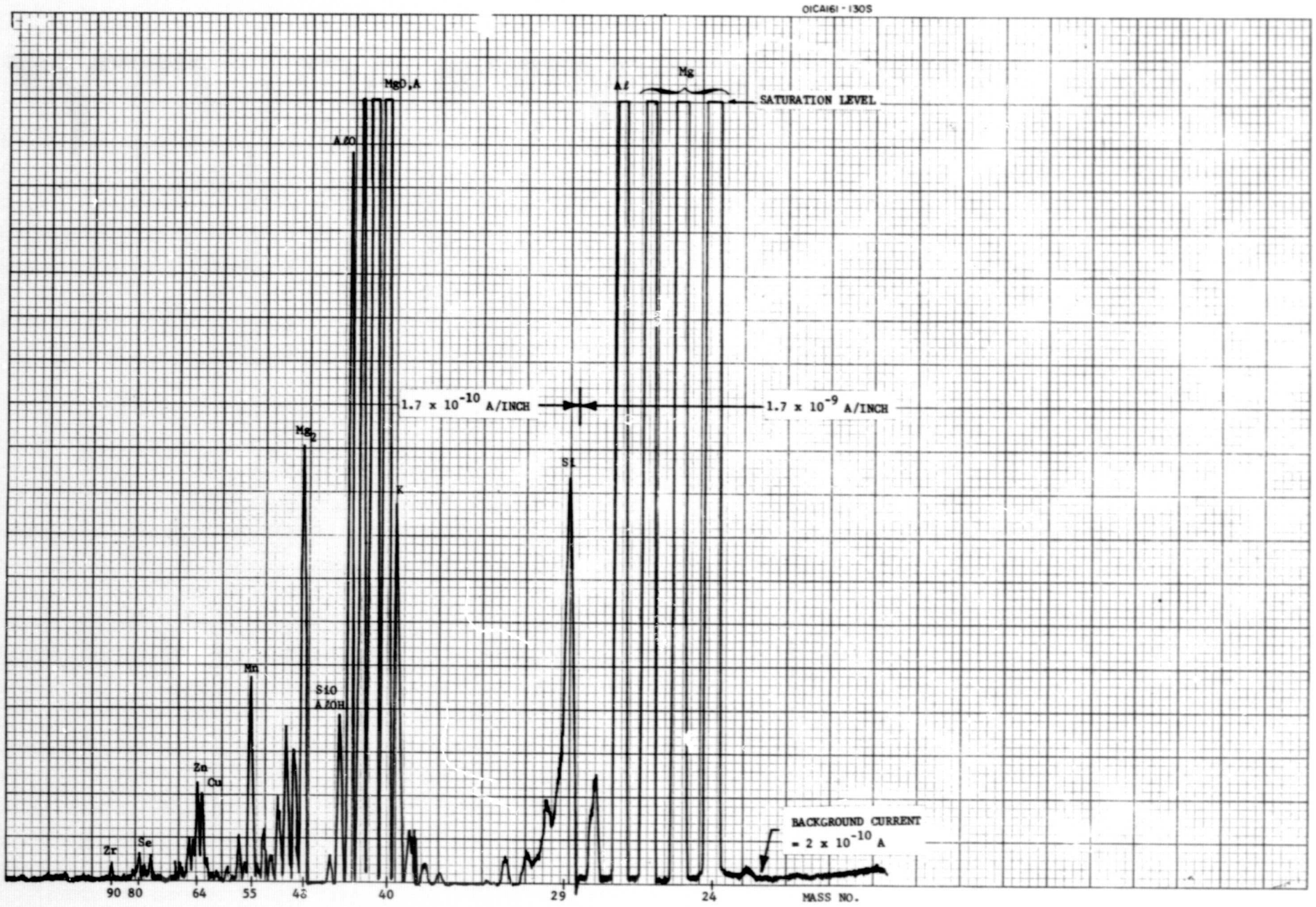

Figure 18. Mass spectrum of magnesium-aluminum alloy.

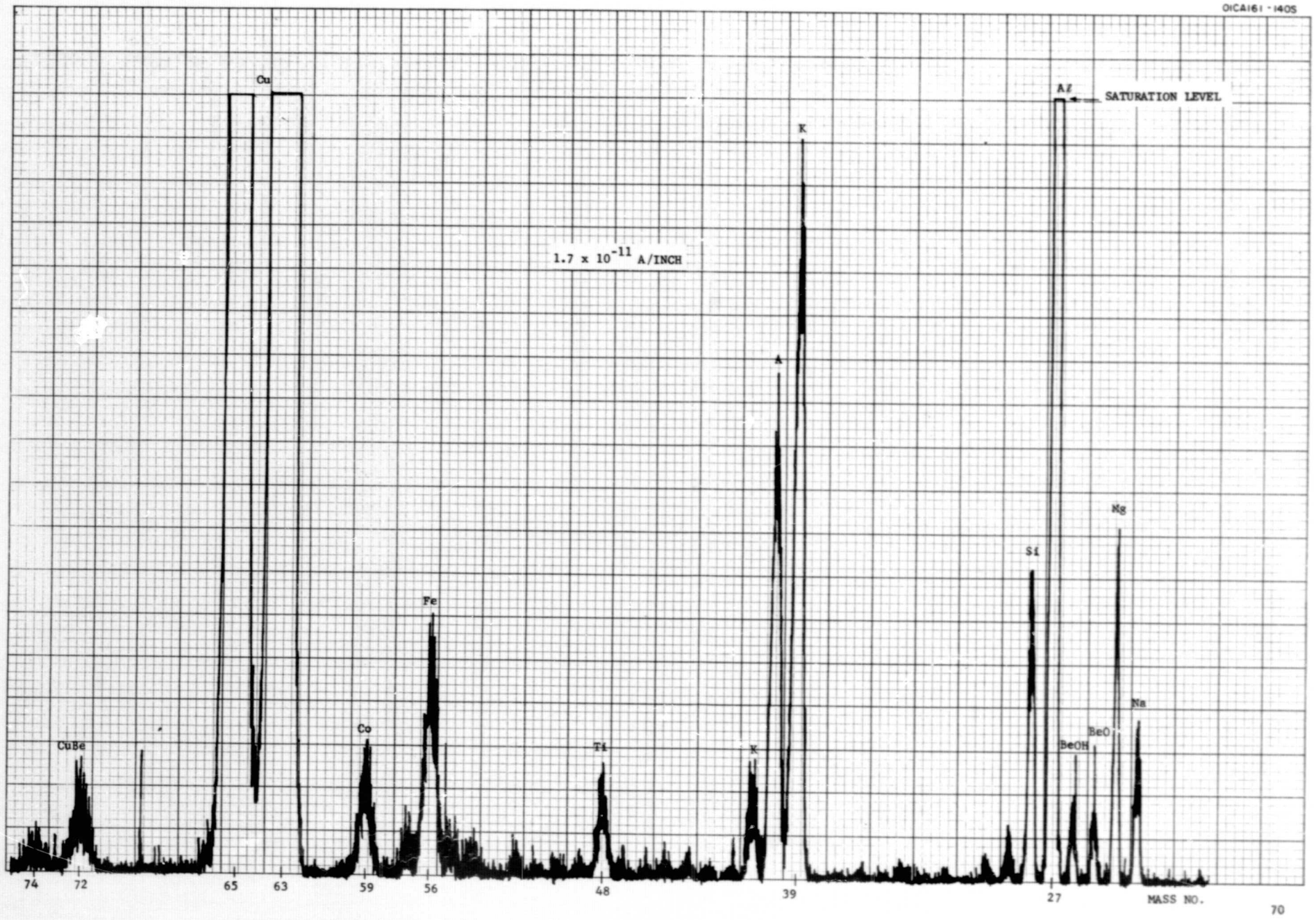

Figure 19. Mass spectrum of copper-beryllium alloy.

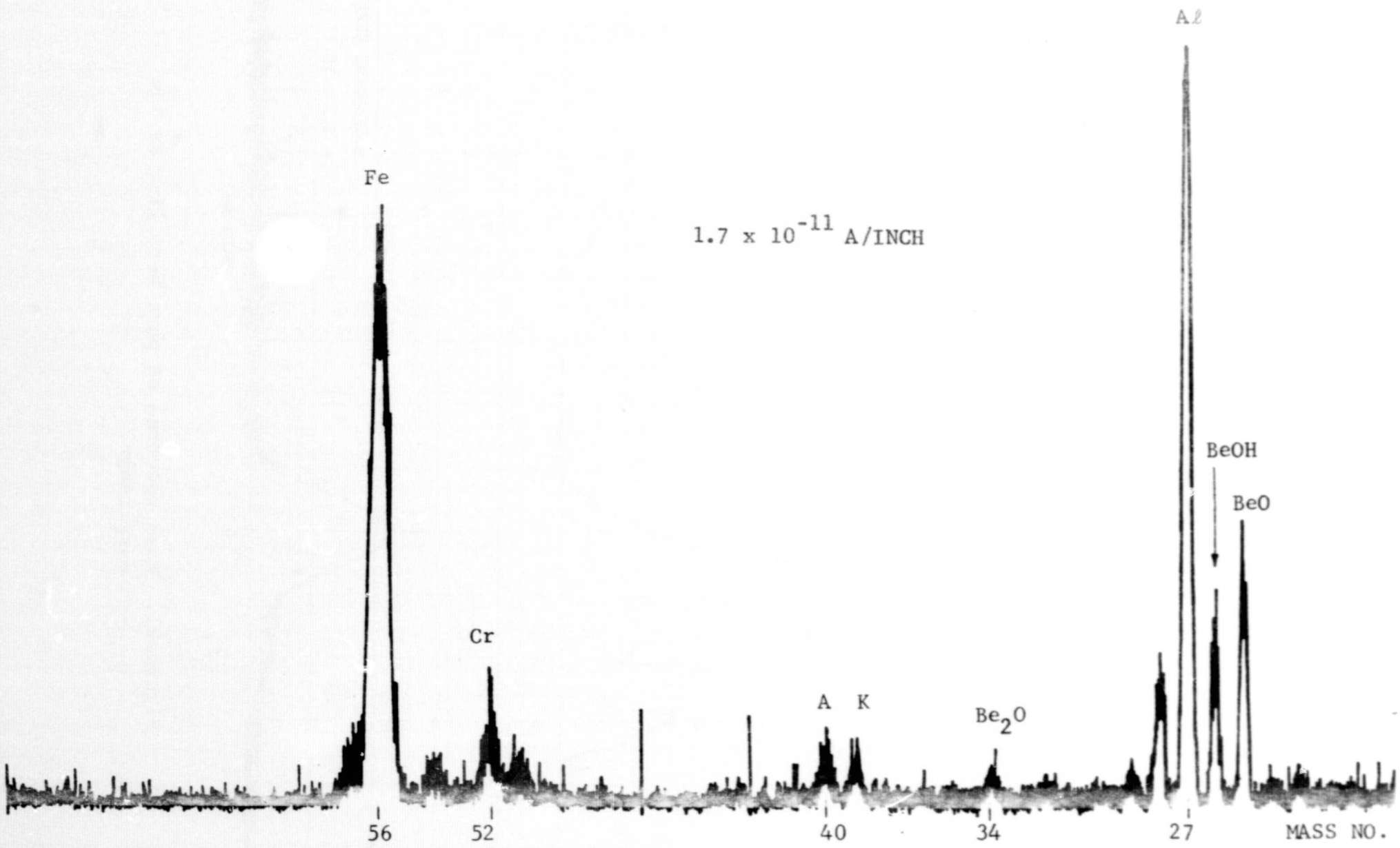

Figure 20. Mass spectrum of pure beryllium on high mass range.

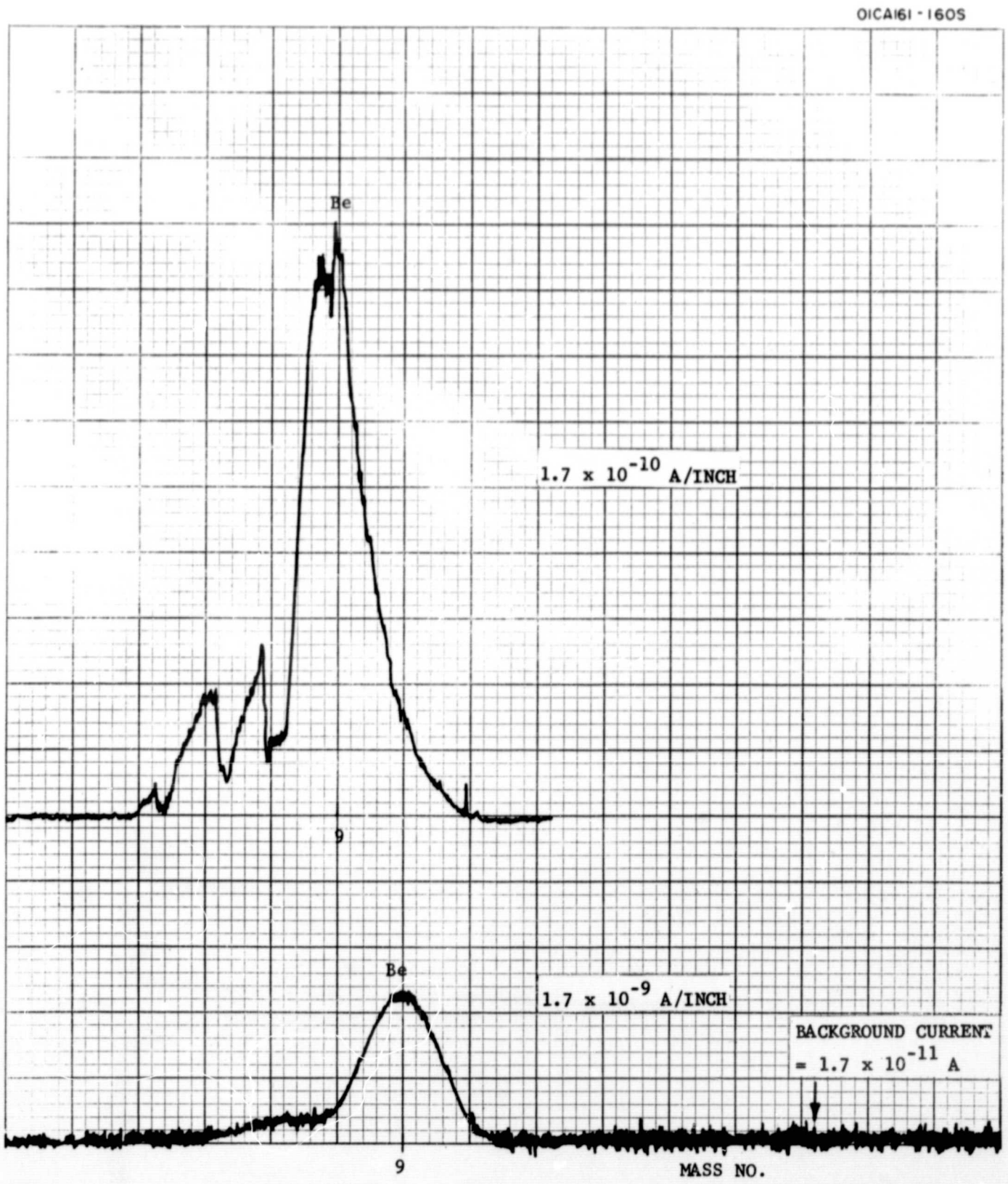

Figure 21. Mass spectrum of pure beryllium on low mass range.

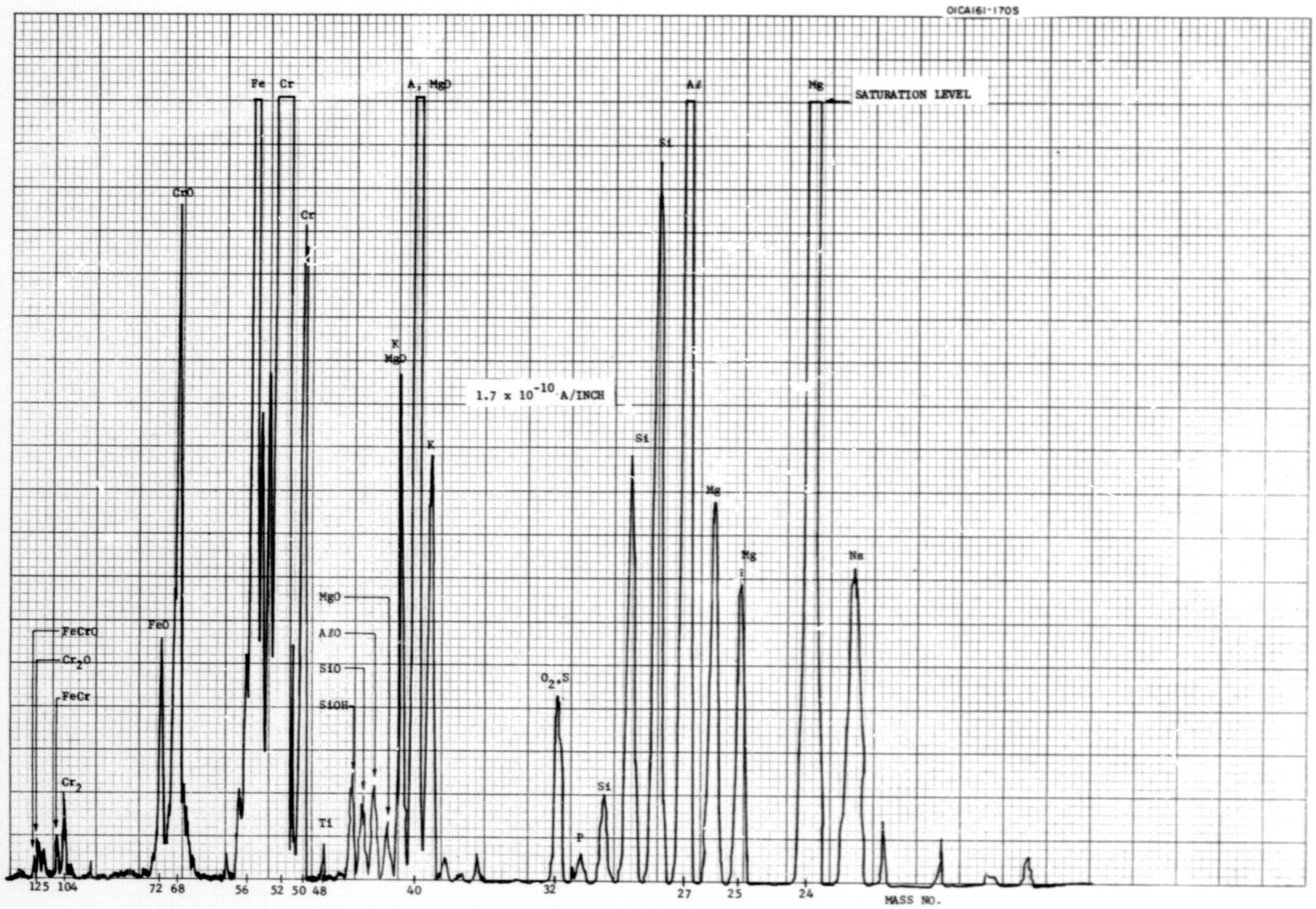

Figure 22. Mass spectrum of 321 stainless steel.

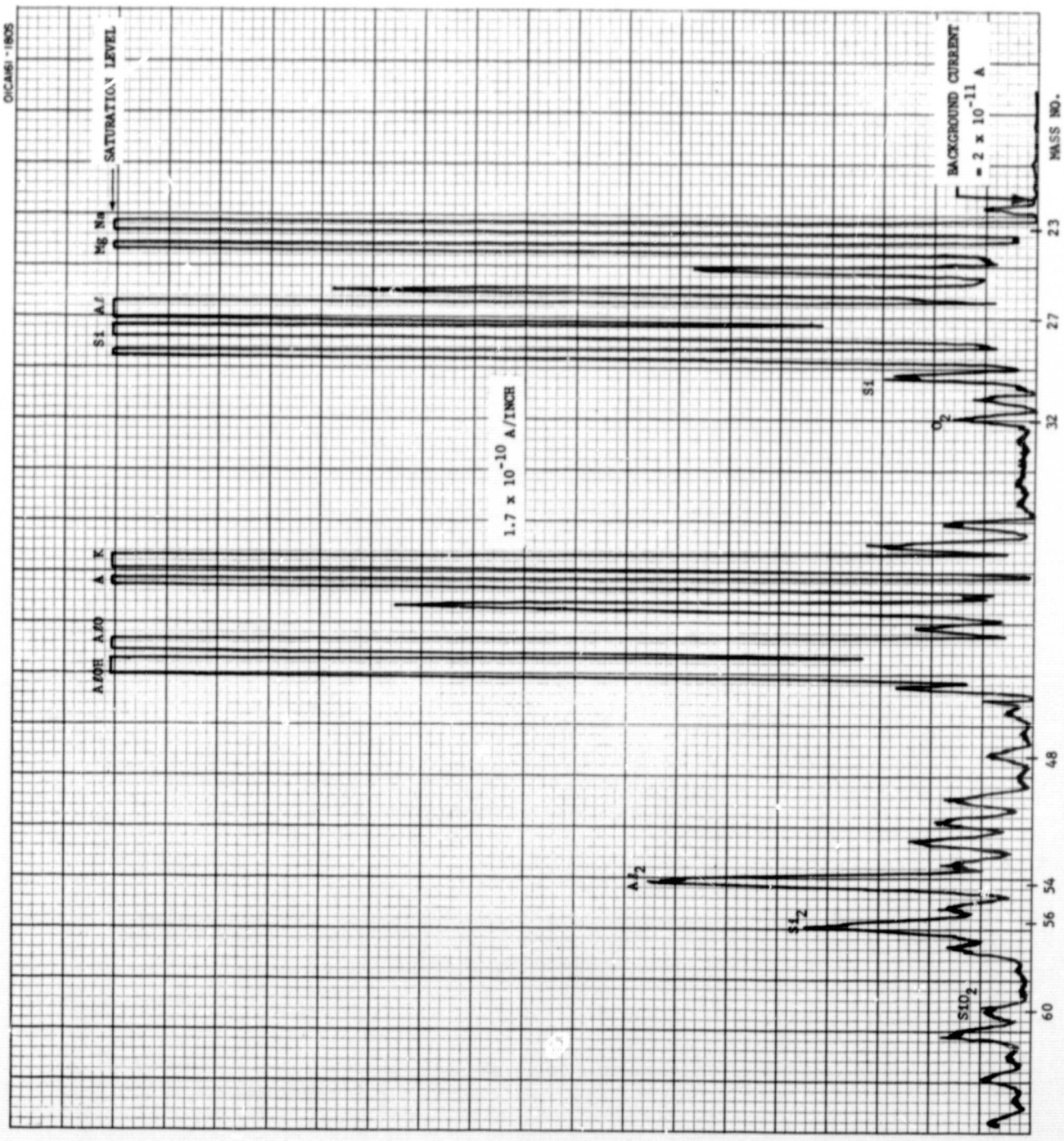

Figure 23. Mass spectrum of pure aluminum oxide.

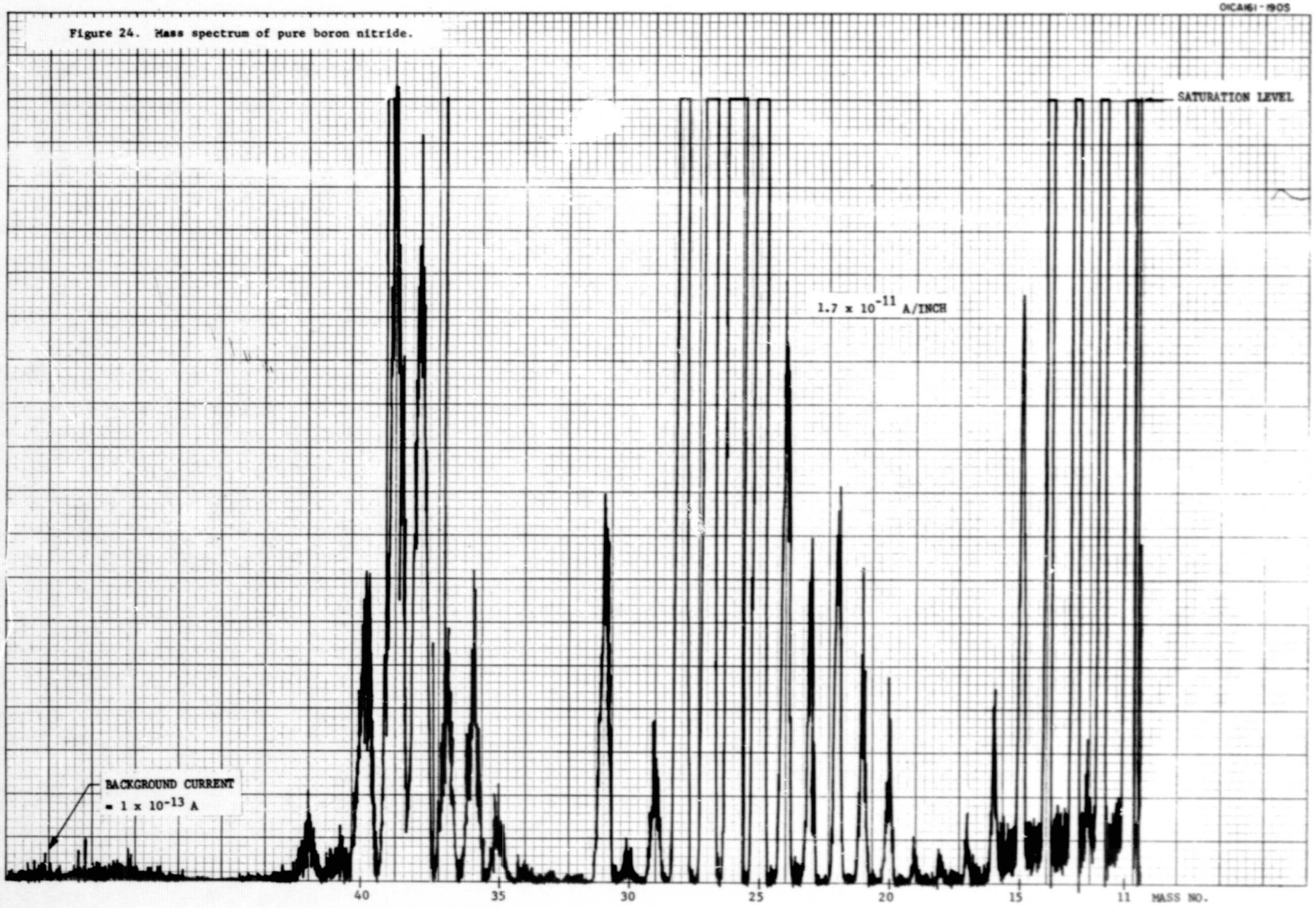

Figure 24. Mass spectrum of pure boron nitride.

secondary ion beam was focused and positioned by a series of electrodes to pass it through a narrow beam width forming entrance slit and a beam angle limiting slit. The formed beam was then passed through a cylindrical electric field (the electric condenser) that allowed only ions with a relatively narrow range of energies to pass through a third slit, the so-called energy slit. The formed and energy homogeneous secondary ion beam was then passed through the magnetic field of the magnetic analyzer sector where momentum separation took place. Ions of different mass were bent into circular trajectories having different radii. Two exit or detector slits were used to define two separate trajectories through the magnetic field. The high mass scale detector slit defined a trajectory having a radius of about 5.5 inches while the low mass scale slit defined a trajectory having a 2-inch radius. "High" mass ions in the range from 10 or 12 amu to 100 amu could be collected simultaneously with "low" mass ions in the range from 1 amu to 10 or 12 amu. Electron multipliers were positioned just behind each of the two detector slits to amplify the small ion currents. The magnetic sector and the high mass electron multiplier were placed on separate movable stages so that they could be adjusted in position while under vacuum.

A vacuum test system was constructed which permitted the entire mass spectrometer to be placed within a metal bell jar that could be pumped down into the 10^{-7} torr region. The mass spectrometer was mounted on a circular base plate, which, in turn, was mounted within a standard feedthrough collar. The various ports of the collar were sealed with flanges containing electrical feedthroughs that permitted various voltages from the electrode voltage control unit and the many power supplies to be connected to the appropriate electrodes of the mass spectrometer. Two of the ports contained motion feedthroughs that permitted the magnet and electron multiplier to be moved while the system was under vacuum and in operation. Argon gas for the primary beam was brought in through the collar also. Three windows were provided in the metal bell jar. The bell jar was pumped down through a 6-inch diameter gate valve and a liquid nitrogen cold trap by a 6-inch mercury diffusion pump backed by a 15 CFM mechanical pump.

Tests made with the lunar lander mass spectrometer revealed that it operated approximately as planned with just a few exceptions. The resolution of the instrument on the high mass "double focusing" scale was 76 based on separation at half peak height when 0.010 inch wide slits were used throughout. Resolution of over 100 could be easily achieved with narrower slits. The sensitivity of the instrument was such that 10 ppm of silicon in 321 stainless steel could be detected. On the low mass scale, the mass peaks of boron 10 and boron 11 were just resolved using a 0.020 inch wide detector slit (the other slits being 0.010 inch wide). The noise and background ion current level at the output of the high mass scale electron multiplier was reduced to 1×10^{-13} amperes by careful shielding. Mass peaks having amplitudes of 10^{-7} and 10^{-6} amperes at the electron multiplier output were generated, and so the instrument had the capability of detecting a few ppm of certain elements such as aluminum and magnesium.

The Penning source proved to be quite stable when operated at a low discharge current of the order of 0.5 mA. Under this condition the source efficiency was low and the sputtering rate corresponding to a sample current of about 5 μA was also low. Although isotope ratios were found to be close to their accepted values, mass discrimination due to the wide range of the swept secondary acceleration voltage was evident. The heavier masses associated with the lower accelerating voltages were reduced in amplitude. When operated with a pure time base sweep, the mass scale was linear.

Problem Areas

The two major problems encountered with the lunar lander mass spectrometer were the charge-up of insulating samples and the poor resolution and sensitivity for low masses.

The charge-up of insulating samples occurred because the neutralization filament was ineffective in getting electrons to the sample surface. The ineffectiveness of the filament was due in part to its location at a considerable distance from the sample but, more important, it was due to the design of the sample holder. Electrons from the filament could easily reach the outer edges of the sample holder, but evidently they did not reach the central recessed portion of the holder where the sample was located.

The poor resolution and sensitivity of the low mass scale was due partly to the fact that this portion of the instrument was not designed to be double focusing. However, the major source of the difficulty was caused by the inhomogeneity of the magnet field through which the low mass ions passed on their way to the detector slit. In addition, the Channeltron electron multiplier was so close to the sector magnet that it was undoubtedly affected by the fringing magnetic field.

Other problems with the instrument were relatively minor ones. They would include such matters as the breakdown of the argon gas in the tube leading to the Penning source, the low efficiency of the Penning source, occasional voltage breakdowns in the electrode voltage control unit, and some unexplained variations in mass peak amplitude with time.

Conclusions and Recommended Instrument Modifications

The lunar lander mass spectrometer was a workable, practical, lightweight instrument that could analyze the various elements in a solid up through mass 100. Even with its low intensity primary ion beam of only a few microamperes, the instrument had sufficient sensitivity to detect trace quantities of the order of a few parts per million of certain elements.

The Penning source proved to be quite stable at low discharge current levels, operating at 750 volts and 0.5 mA (0.375 watts). The efficiency of the source was less than 1 percent which implies that improvement was possible.

The mass spectrometer, including the Penning source, was operated for at least 200 hours during the testing period without any ill effect other than normal darkening of the sample holder, the focus I electrode and the entrance slit where the ion beam impinged.

Although the mass spectrometer was designed to collect both "low mass" and "high mass" ions simultaneously, each mass range was operated separately during the test phase to avoid the requirement for an additional electron multiplier power supply, electrometer and recorder.

The difficulties that were encountered with "charge-up" of insulating samples was due entirely to the poor design of the neutralization filament and sample holder geometry. The standard laboratory sputter source solids analysis mass spectrometer has an effective neutralization filament, and there is no reason why the same cannot be done for the lunar lander instrument.

Problems with the low mass scale of this mass spectrometer could be cleared up by either shimming the present magnetic sector or by changing the shape of the magnetic sector pole pieces. If the Channeltron electron multiplier is adversely affected by the fringing field of the magnetic sector, it can be replaced with a second magnetic electron multiplier.

Instrument memory is a problem with all solids analysis mass spectrometers. Memory effects can be minimized by careful design of the electrodes that are adjacent to the sample holder.

The method of introducing gas into the Penning source should be changed to eliminate the plastic tubing used. The use of glass or ceramic would provide a cleaner primary ion beam. At the same time that this change is made, a flow constriction should be installed at the entrance to the Penning source to reduce the possibility of gas breakdown in the entrance tubing.

The electrode voltage control unit that provided the various operating voltages to the primary and secondary beam electrodes should be modified to avoid the possibility of high voltage arcing and breakdown. Some of the insulators used in this unit were marginal.

Variations in mass peak amplitude that were observed occasionally should be investigated. It is suspected that charged insulating surfaces caused these variations. Quite often such insulating surfaces can be easily shielded from the ion beams.

Finally, it should be recognized that the mass spectrometer that was built was an "engineering model" designed for ease of experimentation and testing. The original version of the instrument was completely unshielded, for example, so that very large stray ion and electron currents completely masked the mass peak signals. In a flight-designed instrument, such shielding would be automatically incorporated in the packaging.

The present engineering model or breadboard lunar lander mass spectrometer has demonstrated the feasibility of building a small (approximately 1 cubic foot), lightweight (approximately 30 to 40 pounds), low power instrument that can operate over the desired mass range of 1 to 100 amu. This mass spectrometer can detect not only the more abundant constituents in this range but also trace elements of a few parts per million. The speed with which the mass scale can be scanned will depend primarily on the electrometer or multichannel analyzer used to process the electron multiplier outputs. The size of the primary beam spot at the sample is of the order of a few square millimeters.

The useful lifetime of the instrument is unknown, but the breadboard version has operated for over 200 hours and the lifetime of the Penning source, one of the critical elements, is certainly much greater than this. The reliability of such a mass spectrometer will depend on the mean time to failure of the electronic components of the various control circuits as well as the Penning source and filament lifetimes (for insulating samples). Memory effects were present and were caused in part by long periods of operation in testing a single sample. Under normal operational conditions, a short sampling time coupled with the low sputtering rate would reduce these memory effects. The spectra of metal samples were quite reproducible and there is every reason to believe that spectra of insulating samples will also be reproducible when the sample "charge-up" problem has been solved.

ACKNOWLEDGMENT

The initial conception and overall ion optical arrangement of a miniaturized sputter source solids analysis mass spectrometer was developed by Dr. R. F. K. Herzog of this laboratory. The design of the primary beam system was carried out by Dr. W. P. Poschenrieder while the design of the secondary beam system was the work of Dr. F. Rudenauer.

REFERENCES

1. Glasstone, S., Sourcebook on the Space Sciences, D. Van Nostrand Co., Inc., Princeton, N. J., 578-9 (1965).

2. Liebl, H. J. and Herzog, R. F. K., J. Appl. Phys., 34, 2893-6 (1963).

3. Herzog, R. F. K. and Poschenrieder, W. P., GCA Technical Report TR-67-6N, GCA Corporation, Bedford, Mass. (March 1967).

4. Langmuir, I. and Kingdon, K. H., Proc. Roy. Soc. (London), 107, 61 (1925).

5. Laegreid, N. and Wehner, G. K., J. Appl. Phys., 32, 365 (1961).

6. Rol, P. K., Thesis, Amsterdam (1960).

7. Almen, O. and Bruce, G., Vac. Symposium Transactions, Vol. 1, Pergamon Press, New York, pp. 245-251 (1961).

8. Almen, O. and Bruce, G., Nucl. Instr. and Math., 11, 257 (1961).

9. Beske, V. H. E., Z. Naturforschg, 19a, 1627-8 (1964).

10. Mattauch, J. and Herzog, R., Z. f. Physik, 89, 786 (1934).

11. Ewald, H., and Hintenberger, H., Methoden and Anwendungen der Massenspektroskopie, Vlg. Chemie GMBH, Weinheim/Bergstrasse (1953).

12. Herzog, R., Z. f. Physik, 89, 447 (1934).

13. Tasman, H. A., Thesis, Rijksumversiteit Leiden (1961).

14. Hintenberger, H. and Konig, L. A., Zs. f. Naturforschung, 12a, 773 (1957).

15. Herzog, R., Zs. f. Naturforschung, 10a, 887 (1955).

16. Wollnik, H. and Ewald, H., Nucl. Instr. and Meth., 36, 93 (1965).

17. Herzog, R., Phys. Zeitschrift, 41, 18-26 (1940).

18. Matsuda, H., Rev. Sci. Instr., 32, 850 (1961).